SISSA - SCUOLA
INTERNAZIONALE
SUPERIORE
DI STUDI AVANZATI
TRIESTE
Strada Costiera 11

ISAS - INTERNATIONAL SCHOOL
FOR ADVANCED STUDIES

A THESIS SUBMITTED FOR THE DEGREE OF MAGISTER PHILOSOPHIAE

EFFECTIVE INTERACTION AND PHASE DIAGRAM OF MACROIONIC SOLUTIONS

Candidate:
Zeenet BADIRKHAN

Supervisor:
Prof. Mario P. TOSI

Academic Year 1987/88

TRIESTE

"بسم الله الرحمن الرحيم"

Dedicated to the memory of my father;

and to my family

ACKNOWLEDGEMENTS

I wish to express my appreciation to my supervisor, Prof. M. P. Tosi for his guidance, continuous support and fruitfull discussions throughout this work.

I would like to thank Dr. M. Rovere for reading the manuscript and discussions.

CONTENTS

CHAPTER I

MACROIONIC SOLUTIONS-PHYSICAL PROPRTIES AND THEORETICAL MODELS

1. Introduction:

Colloid science started with the discovery of mixtures of certain insoluble substances in liquids. In 1845 *Selmi*[1] studied the pseudosolutions in water of *sulpher, silver chloride* and *prussian blue*, and he included them in the same class as solutions of *albumin* and *starch*. *Michael Faraday*[2], by the end of his life, made extensive work on colloidal gold sols (particles of about 3nm radius) called *Faraday sols*, which were prepared by reduction of *gold chloride* with *phosphorus*, *Graham*[3], who coined the term colloid (glue-like), emphasized the low rate of diffusion and drew the correct conclusion that colloidal particles are fairly large.

The colloidal scale is not very precise; colloidal particles should be large enough to have some global average characteristics such as size or shape and at the same time one requires that such particles should be small enough to be subjected to vigorous *Brownian* motion which prevents sedimentation under normal gravity[4].

Some colloidal systems which are thermodynamically stable, called *Lyophilic* (liquid-loving) colloids, contain particles soluble in solvents like polymer solutions. Others, which are called *Lyophobic* (liquid-hating) colloids, contain particles insoluble in the solvent and need the existence of a stabilizing substance during preparation

(e.g. AgCl, Au, S, or oil in water)[5].

Sols have found numerous fundamental applications, as in studies of *Avogadro's* constant by *Perrin*[6], where particles acted as very large, visible molecules; or very recently concentrated colloidal suspensions were used as models for liquid state[7].

The rapid rate of coagulation of colloids was clarified in 1916 by *Von Smoluchowski*[8]: each *Brownian* encounter between two particles results in permenent contact. Refinements to the theory, which take into account that during the last approach between two particles or molecules they are slowed down because it is difficult to squeeze out the last layers of liquid from between them, recently were formulated by several authors[9-12] and confirmed experimentally on the coagulation of latex particles[13]. Phase transition between concentrated liquid-like colloidal dispersions and crystalline arrangements of particles have been observed and discussed theoretically in the framework of the statistical thermodynamics of such systems[14,15].

Colloidal systems have interesting optical properties (colour, turbidity and birefringence), which are also important for applications. Some of these properties are special because the colloidal size lies in the visible-light range of wavelength. Many colloidal particles carry an electric charge due to surface dissociation or to the adsorption of ions: such electric charges are very important in stabilizing colloidal dispersions, in characterizing the particles and their types of interaction which can give rise to crystallization and several other phenomena.

In this chapter we will discuss types of colloids in section 2,

the natural and synthetic colloidal crystals, as well as the experimental methods for studying colloidal systems. In section 3 we will review the types of particle-particle interactions that occur in colloidal suspension starting with the hard sphere interaction, the electrical double layer, *van der Waals* attraction, steric stabilization and ending with the combination of interactions and concentrated systems. Crystallization of colloidal particles will be discussed in section 4, taking into account crystallization under different types of interaction and referring to different theoretical and experimental approaches. The role of *Coulombic* forces in first-order phase transition in the systems of present interest will be focussed upon in section 5.

2. Types of colloids:

Thermodynamically stable colloids of the simplest types are formed by solutions of macromolecules (polymers with 10^4 to 10^8 atoms), including biopolymers such as *proteins, nucleic acids* and *polysaccharides*. All these belong to colloid science since their sizes fall in the colloidal size range (any aggregate of 10^6 to 10^{12} atoms). On account of the great technical importance especially of man-made polymers, polymer science has developed as a science of its own.

The next class of colloids consists of solutions of soaps and other amphipolar substances. These molecules are characterized by a large non-polar part (*hydrocarbon* or *fluorocarbon*) and a water-compatible polar part. The polar part may be anionic, e.g. in

$C_{12}H_{25}OSO_3Na$, or cationic, e.g. in $C_{16}H_{33}N(CH_3)_3Br$, or nonionic as in $C_9H_{19}(C_6H_4)O(CH_2CH_2O)_3H$.

Micelles are particles that are formed from aggregation of 20 or more molcules in water above a certain concentration (the lower, the larger the non-polar part). As the *hydrocarbon* (*flurocarbon*) part is insoluble in water the non-polar groups are driven together, without forming a separate phase because the particle growth stops when the non-polar nucleus is sufficiently surrounded by polar groups, thus minimizing the water-*hydrocarbon* contact area (see fig.1.1). In non-polar solvents the same substance may form the other way around (polar part inside), giving inverse micelles.

Colloidal dispersions of insoluble substances, called *lyophobic* (*hydrophobic*) colloids, are not in thermodynamic equilibrium, but, if well prepared they may have lifetimes of many years. One way of preparing such colloids is known as the condensation method, where the insoluble material is precipitated from solution of small molecules or ions under circumstances in which high rate of nucleation of the new phase is combined with relatively slow rate of growth of the nuclei[5].

The process may be carried out in such a way that the nuclei are formed in a very short time early in the process, whereas the growth to larger particles occurs over a longer time without further nucleation. Under these circumstances all particles grow at the same rate, which leads to monodisperse systems. Monodisperse colloidal particles are capable of forming long-range ordered crystals: these exist in nature and were discovered by *Stanley* in 1935. *Tobacco* and *tomato* viruses (fig.1.2) provide excellent examples of natural monodispersity.

2.1 Natural colloidal crystals:

2.1.1 Viruses: Ordered colloids and colloidal crystals have attracted the attention of physicists for the last forty years, due to their unusual mechanical properties (e.g. *bentonite sols*) or their optical properties. Going back to *Stanley's* discovery, it was followed by the identification of other viruses responsible for a number of animal or plant diseases. These virus particles organize themselves into crystals when concentrated by centrifuging from dilute water suspensions, and can be examined by diffraction method.

It was noticed that rod-shaped particles of *tobacco mosaic* virus (*TMV*) could become parallel to each other and form a two-dimensional triangular lattice. On the other hand, the X-ray study of *Bushy stunt* virus showed the occurence of b.c.c. order for such almost spherically shaped particles. Using a high magnification light microscope *R.C.Williams et al.*[16] reported the discovery of crystalline order in suspensions of *Tipula* virus (fig.1.3). From square and triangular arrays occuring on crystal faces, they deduced an f.c.c. type of close packing of virus particles. The *Tipula* virus crystals when observed by the nacked eye have the appearance of an opal with small regions reflecting the incident light quite brilliantly.

2.1.2. Opals: The precious opals, which sparkle with flecks of pure spectral colour, were examined by X-ray and mineralogical methods, showing that opal is nothing but a hydrated amorphous form of small tiny spherical *silica*, the most common material on earth, cemented

together (fi.1.4).

The voids between the *silica* spheres are filled with a strongly hydrated form of amorphous *silica*. Because of the difference in reflective index between the spheres and voids, the *Bragg* reflection of light makes opals to sparkle (*Darragh et al.*[17]).

2.2. Synthetic colloidal crystals:

Due to pathological properties or rarity, neither opals nor viruses have really been used extensively in physics laboratories. The recent sudden arrival of a huge quantity of results in the physics and physical chemistry of colloidal crystals was brought on by elaboration of very simple, low-cost methods of preparing synthetic monodisperse colloids.

2.2.1. Polymeric monodisperse (*Lyophobic*) colloids: The method of production of such colloids is usually based on free radical polymerization of *vinyl* and/or *butadiene* monomers in an emulsion or solution containing soap or soaplike substances, which act as stabilizers for the polymer. Particles of radius 100nm are formed from a purely chemical point of view the polymerization of monomer M (*styrene*, *methylmethacrylate* ...) in most cases occurs in the presence of an initiator X-X according to the following steps: (fig.1.5)

$T=60\ ^{o}C$

$X\text{-}X \longrightarrow 2X$ free radical formation

$M+X \longrightarrow XM$ initiation

$XM_n + M \longrightarrow XM_{n+1}$ propagation

$XM_n + M_m X \longrightarrow XM_{m+n} X$ termination

The tricky aspects of the emulsion polymerization technique are physicochemical and can be stated briefly as follows: the monomer is insoluble in water, but with the surfactant's help an emulsion will form. The initiator X-X gives free radicals X soluble in water, the initiation and propagations reaction take place in water and end by termination. The solubility of oligomers XM_n decreases rapidly with the length of the insoluble tail M_n, and each of the polystyrene chains starts and ends with an initiator group X. For large n, the solution of XM_n has a tendency towards segregation resulting in the formation of small colloidal particles. Their growth is slow so that statistical dispersion of the number N of incorporated chains decreases with N.

The uniformity of size of such particles depends on many parameters such as the reagent concentration and the physicochemistry conditions of reaction[4].

2.2.2.Silica monodisperse colloids: Several methods of preperation of monodisperse *silica* have been elaborated. One of these was proposed by *Strober et al.*[18](1968): a method of hydrolysis of *alkyl silicates* and subsequent condensation of *silicic* acid in alcoholic solutions, gives very reproducible results provided that the water and *ammonia*

concentration are chosen carefully. In optimal conditions the reaction proceeds rapidly in about three hours, yielding monodisperse *silica* particles about 0.3μm in diameter. If this suspension, prepared without any other treatment, is allowed to stand for a few weeks in a glass recipient then an opal-like sediment will form at the bottom.

The choice of physicochemical conditions for the reaction is tricky in the sense that if all input products of reaction are soluble in alcohol at certain concentrations, then amorphous *silica* is the result of condensation of *silicic* acid groups. Since the *silicon* atoms are tetravalent, a three dimensional network of $(SiO_2)_n$ macromolecules is built up, which is stiff and more solid than a coil of polymer chains. Due to this fact *silica* particles do not dissolve in organic nor in most inorganic solvents[4].

2.3. Experimental methods for studying colloidal system:

Various experimental techniques are used in order to study colloidal solutions. In particular, owing to the length scale involved in these systems, the properties of colloidal dispersions can be studied optically. In this section we will give some examples of different types of experimental methods used to study the structure of dilute and concentrated solutions.

2.3.1. Light scattering: The theoretical devolepment behind light scattering studies goes back to more than a centuries, with notable contributions from *Maxwell*, *Rayleigh*, *Einstein*, *Mie*, *Deby* and many others. The experimental development of conventional (time averaged)

light scattering started around 1940: basically, one measures the absolute intensity of light scattered by the suspension as a function of scattering angle. In 1961 great progress of light scattering techniques was brought about by the invention of the laser, an intense and well-collimated light source. This led to the development of a totally new technique, i.e. dynamic light scattering, providing information about the dynamics (i.e. the *Brownian* motions) of the particles in colloidal suspension. In what follows a breif outline is given of conventional light scattering followed by a description of dynamic light scattering.

The scattering of light by independent particles can be divided into three classes[19]:

(i) *Rayleigh* scattering, where the scattering particles are small enough to act as point sources of scattered light;

(ii) *Debye* scattering, where the particles are relatively large and there is small difference between the refractive index of the particles and of the dispersion medium;

(iii) *Mie* scattering, where the particles are relatively large and their refractive index differs significantly from that of the dispersion medium.

2.3.1a. Conventional light scattering[20]: The electric field is associated with a beam of light incident on a colloidal suspension, which oscillates at frequency $\upsilon=c/\lambda$, where c is the velocity of light and λ the wavelength in the suspension. As there is a difference between the refractive index n_1 of the particles and that of the medium n_2, this electric field induces in a particle a dipole moment which

also oscillates at frequency υ and hence causes a reradiation or scattering of the light in all directions. Assume the electric vector of the incident light to be polarized perpendicular to the scattering plane, the scattering radiation with this same polarization is observed at a detector set at scattering angle θ, at a distance r from the sample. The intensity I_R of light scattered by an isolated particle of size R much smaller than λ (i.e. *Rayleigh* scattering) is

$$I_R = \frac{16\pi^4}{r^2} \frac{R^6}{\lambda^4} \left(\frac{n_1^2-n_2^2}{n_1^2+n_2^2}\right)^2 \quad . \qquad (1.1)$$

We can see that I_R is independent of the scattering angle θ. It depends on the refractive indeces $n_1$and n_2, it si zero for $n_1=n_2$, and goes as λ^{-4}, the well known *Rayleigh* scattering law.

In the second class,i.e. *Debye* scattering, the electric field scattered at nonzero angle θ from different parts of a particle, whose size is comparable to λ, will suffer relative phase shifts. Thus interference between the different element scattered fields occurs at the detector and the scattered intensity is reduced relative to I_R in eq.(1.1). Then the intensity measured here in the *Debye* limit $[(n_1-n_2)R/\lambda \ll 1]$ is

$$I_D = I_R . P(\theta) \quad , \qquad (1.2)$$

where $P(\theta)$ is a shape factor with properties $P(\theta=0)=1$, $P(\theta>0)<1$ for a homogenous sphere. Its form is

$$P(\theta) = \left[3(\sin QR - QR\cos QR)/(QR)^3\right]^2 \quad , \qquad (1.3)$$

where Q is the scattering vector given by

$$Q = (4\pi/\lambda)\sin(\theta/2) \quad , \qquad (1.4)$$

when the *Debye* limit is not fulfilled, i.e. in the *Mie* scattering class, the incident light wave can be distorted on passing through the particles and the theoretical situation is more complicated. For very large particles ($R \gg \lambda$), a complex angular dependence of scattered intensity is found and the angle-dependence of the intensity is a very sensitive measure of particle size and structure.

2.3.1b Dynamic light scattering[20]: The devolepment of dynamic light scattering followed the invention of laser. The important property of laser light is that it is coherent so that phase relationships are maintained in the scattering process. Hence the particles in a suspension can be regarded as forming a random three-dimensional diffracting array which gives rise to a random diffraction consisting of small bright spots (largely constructive interference) and dark areas (where destructive interference occurs). The particles suspended in the medium are not stationary but having a *Brownian* motion caused by collisions with the thermally agitated medium molecules. The phase relationships, determining the diffraction, reflect the movement of the particles and the pattern itself changes continously through a series of random configurations. Thus the detailed nature of temporal fluctuations in the scattered intensity contains information on the particle motions.

2.3.2 Dilute and concentrated suspensions: For sufficiently low concentration, the position of particles in a suspension are

essentially uncorrelated. Using conventional (incoherent) light the intensities scattered by different particles are simply added at the detector whereas with a coherent (laser) source, temporal fluctuations are observed in the scattered intensity; however if this intensity is averaged over many fluctuation times it is again simply the sum of the intensities scattered by individual particles.

For a concentrated suspension, in X-ray scattering, laser scattering and other types of experiments a broad single peak in the small angle region is observed, where the peak has been taken to suggest that the solute macroions form an ordered strcture in the solutions[21]. There is a close formal analogy between the random diffraction pattern formed by laser light scattered by particle suspension and the diffraction pattern of X-ray scattered by a crystal. The main difference is that the atoms in crystal are constrained to the neighbourhood of sites of a regular lattice; thus the diffraction pattern consists of an ordered array of spots whose intensity hardly fluctulates. Secondly, when a particle suspension is illuminated by light from a conventional source, due to its lak of coherence, phase relationships are only maintained over few interparticle spacings rather than over the whole scattering volume.

2.3.3 Experimental work: The crystal structure of an ordered suspension of polystyrene spheres was determined using *Bragg* scattering of laser light. At low concentrations a body-centered-cubic structure is found, whereas both body-centered and face-centered structure are found at high concentration. In table 1.1 the lattice constant (microions) as a function of latex sphere density $N(cm^{-3})$ is given

where both experimental measured value and calculated value are presented[22]. The intermolecular ordering distance $2D_{exp}$ was calculated using the *Bragg* equation by analysing the small angle X-ray scattering measurements and it was found that $2D_{exp}$ decreases with increasing polymer concentration and the values obtained were smaller beyond experimental error than theoretical distance $2D_o$ calculated from the concentration by assuming uniform distribution of macroions throughout the solutions. Figure (1.6) shows typical scattering curves of *sodium salts* of polystyrene *sulfonate* (NaPSS) at various polymer concentrations as a function of scattering vector, and in table (1.2) some of the data are shown which are related to the same figure (Fig.1.6)[23]. We shall return to a discussion of theoretical developments related to these observations at the end of this chapter.

Among different methods of crystal structure determination by light diffraction, the *Kossel* technique is probably the most direct one. The *Kossel* lines observed in colloidal crystals are similar to those in X-ray diagrams. With a point source of monochromatic light situated close to the colloidal monocrystal, consider a family of lattice planes (hkl) and a light ray incident on these planes. At the *Bragg* reflection angle θ (for a given light wave length λ) one expects that due to *Bragg* reflection the transmitted light intensity will be different from other rays which do not satisfy the *Bragg* condition. All rays incident on the plane (hkl) at the same *Bragg* angle θ will form the *Kossel* cone with axis [hkl] and cone angle $\mu=\pi/2-\theta$ (Fig.1.7).

The *Kossel* line is an intersection of the *Kossel* cone with the projection screen, and the set of *Kossel* lines on the projection screen forms the *Kossel* diagram[4]. The analysis of *Kossel* lines of highly

charged polystyrene paricles in semidilute aqueous solutions was made by *T.Yoshigama et al.*[24](Fig.1.8) in an invastigation of the properties of these colloidal crystals which have typically lattice spacing of order of visible-light wave lengths. The lattice constant were again found to be systematically smaller than those calculated from uniform particle distribution throughout solution (table 1.3). It is interesting also to note that only the intensity of *Kossel* lines decreases as a function of their *Miller* indices whereas their angular width does not change with $(h^2+k^2+l^2)$: this shows that the crystal ordering is of long range.

By *Bragg* reflection of visible light, an aqueous colloidal suspensions of charged polystyrene microsphere was studied by *Aastuen et al.*[25] body centered cubic crystalline were shear melted into the metastable liquid phas. Recrystallization occurs via nucleation and growth of single crystallites at dilute sites with nearly spherical growing crystals (Fig.1.9).

The small angle neutron scattering (SANS)[26] is also one of the experimental techniques used to study different properties of the atomic order to obtain information about various parts of the particle and to study for example, molecules absorbed on the particles. For this reason SANS offers many advantages over the more conventional light scattering (i.e. a shorter wave length is needed for such studies). *Ghuan-Fu Wu et al.* had used the SANS technique to study concentrated proteins in mixed D_2O/H_2O solutions: they extracted from the data three basic properties, the dry volume, the hydration, and the amount of H/D exchange of the protein in D_2O-containing solvents.

3. Types of particles-particle interaction:

In this section we will introduce at a qualitative level some elementary notions on the different interaction models that are relavant to colloidal particles. We shall also mention highly charged particles in suspension, that we shall be dealing with in more detail later.

In a sol with a low concentration of particles in an intermediate electrolyte, the particles are allowed to move freely in the large volume of the dispersion medium. Such *Brownian* motion involves translational diffusion of particles. In such dilute dispersions only occasional contacts occur between the particles. Hence, as was examined experimentaly by *Perrin* and theoretically by *Einstein* in the early days of the twentieth century, the diffusional motion is only very marginally restricted.

As the number concentration of the sol increases, the probability of interactive contact between particles increases, since the volume of space occupied by the particles relative to the total volume increases. It is in such situation that the forces between particles play an important role in determining the overall properties of the dispersion[27].

It is coustomary and to some extent useful to discuss the different types of interactions which can occur between particles in terms of the energy of interaction between a pair of particles as a function of the distance separating their centres. Then considering only spherical particles having radius a, say, and separated by a

distance R, we will discuss the different types of interaction in brief, keeping in mind the following; the actual volume of a particle, v_p, is given by

$$v_p = \frac{4}{3}\pi a^3 \quad , \qquad (1.5)$$

and the total volume of N_p particles in the system is υ:

$$\upsilon = N_p v_p \quad , \qquad (1.6)$$

with the total volume of dispersion taken to be v. The actual volume fraction is $V=\upsilon/v$.

3.1 Hard sphere interaction:

It is the simplest model, as one thinks of colloidal particles as hard and electrically neutral. At a certain distance of separation, R′, the energy of interaction rises very steeply to infinity, hence (Fig.1.10)

$$R' = 2a_{Hs} \quad , \qquad (1.7)$$

where a_{Hs} is in general greater than the physical radius of a single particle, but in some cases is close to it. Then from a theoretical point of view, the hard sphere system is described by a dimensionless parameter V_{Hs}, the excluded volume fraction, defined as

$$V_{Hs} = \frac{\upsilon_{Hs}}{v} \quad , \qquad (1.8)$$

with υ_{Hs} the total volume of particles with radius a_{Hs}. It is clear

that $V_{Hs}>V$ since a_{Hs} is greater than the actual radius.

3.2 Electrical double layer repulsion:

The majority of colloidal particles have an electrical charge on the surface, which will give rise to a surface electrostatic potential ϕ_s [28], and to a potential energy of electrostatic ϕ_R. For small spherical colloids one usually writes (Fig.1.11)

$$\phi_R = \frac{\epsilon_r a^2 \varphi_s^2 \exp[-\kappa(R-2a)]}{R} \quad , \qquad (1.9)$$

with ϵ_r the relative permittivity of the medium, and κ the reciprocal *Debye-Huckel* electrical double layer thickness, which is related to the concentration of symmetrical electrolyte c by

$$\kappa^2 = \frac{Z^2 e^2 N_A c}{\epsilon_r k_B T} \quad , \qquad (1.10)$$

Here, Z is the valency of the ions, k_B the *Boltzmann* constant, T the absolute temperature and N_A *Avogadro's* number.

It is clear from eq.(1.5) that the change in the interaction energy with R is dependent on the term $\exp[-\kappa(R-2a)]/R$, and the rate of decrease of repulsion with distance is strongly dependent on κ. Then at low electrolyte concentrations, the electrostatic repulsion provides a long range term whereas at high electrolyte concentration the repulsion energy decays rapidly.

The force of repulsion between particles is determined by the gradient of ϕ_R. It can be seen from fig.(1.11) that the repulsive force

becomes so strong at certain distance of approach that any closer approach is improbable. This provides the useful concept of the effective radius: the particles can be viewed as hard spheres with an effective radius that is larger than the actual radius.

3.3. Van der Waals Attraction:

The explanation for attractive (*Van der Waals*, or dispersion) forces between neutral particles was given by *London* in 1930[29]. The instantaneous dipole μ on one particle generates an electric field E, which has a strength of order μ/R^3 at distance R. If there is another particle at this point the field polarises it and creates a dipole μ_1 of strength $\mu_1=\alpha E$ where α is the polarizability of the particle. The field at the first particle thus is of order μ_1/R^3 and hence the two particles interact via a potential

$$\phi = -C/R^6 \quad , \qquad (1.11)$$

where C is a constant characteristic of the particles in the system. *London* solved the problem for the simplest case of two atoms.

The interaction ϕ_A between two spherical particles of equal radius was originally given by *Hamaker*[30] in the following (fig.1.12);

$$\phi_A = \frac{-A}{12}\left[\frac{1}{x^2+2x} + \frac{1}{x^2+2x+1} + \frac{x^2+2x}{x^2+2x+1}\right] \quad , \qquad (1.12)$$

where x=(R-2a)/2a. A is the composite *Hamaker* constant for the particles in the medium, given by

$$A = (A_{11}^{1/2} - A_{22}^{1/2})^2 \quad , \qquad (1.13)$$

with A_{11} the *Hamaker* constant of the particles and A_{22} that of the medium. In general the *Hamaker* constant is defined as;

$$A_{123} = \sum_i \sum_j q_{i1} q_{j3} \lambda_{i2j}$$

where q_{i1}, q_{j3} are number of i or j atoms per unit volume in the material 1 and 3 of the two particles; λ_{i2j} is their interaction parameter in the medium material 2.

3.4 Steric stabilisation:

The tendency of particles to aggregate in a colloidal dispersion is the most important physical property of such dispersions. Encounters between particles dispersed in liquid media occur frequently and the stability of dispersion is determined by the interaction between particles during these encounters.

If the *Coulomb* effects between particles are not important, then the main reason for aggregation is the *van der Waals* attractive forces between particles, whereas stability against aggregation is a consequence of repulsive interactions between similarly charged electric double layers and particle-solvent affinity. Particle-solvent affinity promotes stability mainly by mechanical means, which can be considered in terms of the positive desolvation free energy change ΔG_{des}, which accompanies particle aggregation (i.e. a stabilizing mechanism; steric stabilization)[19].

The name steric stabilisation is commonly used to describe several different possible stabilizing mechanisms involving absorbed macromolecules, such as desorption of stabilizing agent with negative free energy change ΔG_{ads}. Desorption with positive free energy change ΔG_{des} correspond to particle-particle repulsion and enhanced stability.

Whenevere specific *Coulomb* effects are unimportant, *van der Waals* attraction plus hard sphere repulsive potentials are a resonable model to decribe colloidal dispersions. The forces between sterically stabilized particles have been measured and have been shown to be short range, with a range comparable to twice the contour length of the *Lyophilic* chains. For sterically stabilized systems the total interaction energy can be written as

$$\phi = \phi_A + \phi_s \quad , \qquad (1.14)$$

where ϕ_A is the *van der Waals* potential, ϕ_s is the steric potential that can be considered for simplicity as a hard sphere interaction with an effective radius a plus the thickness of the absorbed layer δ (fig.1.13).

3.5 The combination of interactions and concentrated systems:

In the real world it is possible to obtain colloidal dispersions in which various combinations of different interactions occur. A schematic picture of particle arrangements is shown in fig.(1.14).

If the repulsive forces are the dominant ones, there is a strong

dependence on the range of repulsion a_{eff}. As we increase the number of particles, then each particle will interact with others with the consequent formation of a dispersion with high degree of order: in such system each particle will have a high coordination number, which could approach 12 as in the formation of an f.c.c. array. The particles are still separated by the dispersion medium, though forming an ordered system (crystal or solid phase). Thus in the case of aqueous dispersions at low electrolyte concentration, a_{eff} can be greater than a.

In a concentrated dispersion, when the attractive force now is the dominant one, the particles will stick on coming into an attractive energy well, with a result of formation of highly disordered system (fig.1.14b) with high void volume and low coordination number for each particle[27].

In what follows we will discuss crystallization that might occur in colloidal suspension from experimental and theoretical points of view.

4. Crystallization of colloidal particles:

Different crystallization processes are possibble because of the different types of interaction, mentioned in the previous section, that can occur between colloidal particles in suspension. From purely thermodynamic considerations solid-liquid coexistence is characterized by

$$T_s = T_l \quad ; \quad P_s = P_l \quad ; \quad G_s(P,T) = G_l(P,T) \quad . \qquad (1.15)$$

These three conditions correspond to thermal equilibrium, mechanical equilibrium and chemichal equilibrium between the two phases (s≡solid, and l≡liquid). Each of the quantities, temperature, pressure and the *Gibbs* free energy per particle, must take the same value in the solid phase as in the liquid phase.

With present-day computers one can simulate accurately the properties of a few thousand interacting particles and obtain accurate values for thermodynamic properties over the whole density range. But the difficulty still remain of knowing what the forces in real materials actually are.

In this section, we are going to discuss some crystallization models for different types of interaction between the particles and we will start with the simplest idealization of intermolecular forces, the hard sphere potential.

4.1 Crystallization under purely repulsive forces approaching the hard sphere potential:

In the general case of the inverse-power repulsive potential given by

$$\phi(r) = \epsilon(\sigma/r^n) \qquad , \qquad (1.16)$$

the particles are considered as point centers of repulsion with the force on any particle being a vector sum of contributions $-d\phi/dr$ from all the other particles. The strength of the interaction is measured by

a microscopic energy ϵ. The diameter of the particles is the length σ and the hardness or stiffness of the particles increases with n. For the *Lennard-Jones* potential n=12, while n=∞ for the hard sphere model.

For any of the inverse power potentials the thermodynamic properties are easy to calculate because once a single isotherm, isochore or isobar is known all the others can be determined from it. This follows from the way that the configurational *Helmholtz* free energy depends on the density and temperature. The *Helmholtz* free energy H=U-TS, rather than the *Gibbs* free energy function G=U-PV-TS=H+PV, is more convenient in statistical calculations because volume (rather than pressure) is the convenient independent variable in theoretical calculations. From statistical mechanics the dependence of the *Helmholtz* free energy on the volume and temperature is given by the canonical partition function $Z_N(V,T)$[31]:

$$Z_N = \exp(-H/k_BT) = \frac{1}{N!\Lambda^{3N}}\int \exp(-\sigma^n \frac{\epsilon}{k_BT} \sum r_{ij}^{-n})\, dr^N$$

$$= \frac{V^N}{N!\Lambda^{3N}}\int \exp(-\rho^{n/3} \frac{\epsilon}{k_BT} \sum s_{ij}^{-n})\, ds^N \quad , \qquad (1.17)$$

where

$$\rho=N\sigma^3/V \quad ; \quad s=r(N/V)^{1/3} \quad ; \quad \text{and} \quad \Lambda^2=h^2/(2\pi mk_BT) \quad .$$

The sum is over all N(N-1)/2 pairs of particles. The reduced distances {s} have been introduced to show that the non-ideal part of the free energy, given by the integral multiplying $V^N/(N!\Lambda^{3N})$ in eq.(1.17), depends only on the single density-temperature variable $\chi=\rho(\epsilon/k_BT)^{3/n}$, rather than on V and T separately. This remarkable simplification of the partition function occurs only for invers power potentials.

Along any isotherm, isochore or isobar the liquid-solid transition is characterized by discontinuities in $(\partial P/\partial V)_T$, $(\partial P/\partial T)_V$, $(\partial T/\partial V)_P$ respectively. In order to locate the phase transition, in a computer experiment the pressure or energy data for the two phases have to be integrated to get the free energy. The *Helmholtz* free energy for each phase can be determined by either a volume or a temperature integration, using

$$(\partial H/\partial V)_T = -P \quad ; \quad (\partial [H/T]/\partial T)_V = -U/T^2 \qquad (1.18)$$

then the phase boundaries, along which the solid and liquid temperature, pressure and *Gibbs* free energy per particle are equal, can be determined. Note that the inverse power repulsive potentials are the simplest to use, but not sufficiently realistic at low temperatures. More importantly, attractions must be taken into account in order to find that the fluid phase admits in fact two phases, namely liquid and gas. This is shown in fig.(1.15) in which the *Lennard-Jones* density-temperature phase diagram[31] is plotted and has superimposed on it the phase diagram for the purely repulsive soft-sphere model (with n=12).

In the simulation of the hard-sphere model by *Hoover* and Ree[32] two different phases are demonstrated, using a thermodynamical reversible path linking the solid and liquid phases with a periodic external field to stabilize the solid phase at low density. Define the volume fraction as $\Phi=nv$ where n is the number of particles per unit volume and v is the volume of one particle, and the reduced pressure $P^*=P/n_{cp}k_BT$, where $n_{cp}=\Phi_{cp}/v$ is the density of close packing limit (Φ_{cp}). Crystallization occurs at $P^*=8.27$ for liquid phase

(topologically disordered phase) of volume fraction Φ_1 equal to 0.50 in equilibrium with a solid phase (long range ordered phase) of Φ_s equal to 0.55 (fig.1.16).

According to this model crystallization will occur in a concentrated suspension with volume fraction larger than 0.5. Unfortunately in experimental techniques for preparation of polymers the concentration of monomer or the *silicic acid esters* must be less than 10% in weight, otherwise the particles in suspension would stick during the reaction and the suspension would floculate (fig.1.14).

The desired densification may be obtained by other methods such as sedimentation.

4.2 Sedimentation studies:

To see how sedimentation comes about, consider a particle of volume v and density ρ_2 which is submerged in a fluid of density ρ_1 and is under the influence of gravitational forces. The particle experiences a force F_g due to gravity (positive in the downward direction); at the same time a buoyant force F_b acts in the opposite direction. A net force equal to the difference between these forces results in acceleration of the particle:

$$F_{net} = F_g - F_b = v(\rho_2 - \rho_1)g \qquad (1.19)$$

This force will pull the particle downward, that is if F_{net} will have the same sign as g, if $\rho_2 > \rho_1$, and the particle is said to sediment. On the other hand if $\rho_1 > \rho_2$ then the particle will move upward, which is called creaming.

Consider a cylindrical container filled with a monodisperse

colloid, with a relative density of colloidal particles $\bar{\rho}=\rho_{coll}-\rho_{sol}$, where ρ_{coll} and ρ_{sol} stand for the densities of the solid and liquid contents of the colloid. Let dz be the thickness of a layer in the container, which is under the influence of a gravitational force per unit area (fig.1.17) given by

$$dP = -\bar{\rho}g\Phi dz \quad , \qquad (1.20)$$

where Φ is the volume fraction at pressure P and satisfies the equation of state of two phases, the solid and liquid phase, as

$$\Phi = \Phi_l(P^*) \quad ; \quad \Phi = \Phi_s(P^*) \quad , \qquad (1.21)$$

combining equations (1.20) and ((1.21) on gets the differential equation

$$\frac{dP^*}{d\bar{z}} = \bar{\Phi}(P^*) \quad , \qquad (1.22)$$

with dimensionless variable $\bar{z}=z/h_o$, where $h_o=k_BT/v\bar{\rho}g$ and $\bar{\Phi}=\Phi/\Phi_{cp}$. Knowing $\bar{\Phi}(P^*)$ from equation (1.21) on gets by integration

$$\bar{z} = -\int_{P^*_{crit}}^{P^*} \frac{dP^*}{\bar{\Phi}(P^*)} \quad , \qquad (1.23)$$

with $\bar{z}=0$ at the interface between the solid and liquid phases and $P^*_{crit}=8.27$ from *Hoover* and *Ree*. We can see that at the top of the liquid phase the pressure decreases exponentially with height, according to the perfect gas approximation valid at very high dilution,

$$P^* \sim \exp(-\bar{z}) \quad . \qquad (1.24)$$

The overall hight of liquid phase above the solid-liquid interface is of order h_o. Now with $\bar{\rho}=50$ Kgm^{-3} (*polystyrene* in water) and T=300 K one

gets h_o in the range 1.6cm-16μm for 0.1μm<2a<1.0μm. For *silica* particles in water $\bar{\rho}=10^3 Kgm^{-3}$ so that h_o is reduced by a factor of 20.

The sedimentation method is an experimental technique by which one is checking the validity of crystallization of the hard sphere system provided that the column (fig.1.17) is sufficiently high, and that sedimentation equilibrium is obtained, keeping in mind that the time needed to have equilibium in a coulmn of height h is of order

$$\tau_{sed}^{min} \simeq h/u_{sed} \quad , \qquad (1.25)$$

where $u_{sed} \simeq v\bar{\rho}g/(6\pi\eta a)$, as calculated from *Stokes* formula in a liquid of viscosity η. Then a month is needed to attain sedimentation equilibrium in a test tube of a few centimeters hight containing *polystyrene* latex, and might reach one year in other experiments. *Takano et al.*[33] in their experiment attempted to measure the pressure using the sedimentation method for monodisperse latex. A phase transition phenomenon from an ordered state to a disordered state was achieved. The transition pressure, P_m, expressed in terms of the reduced pressure, $P_m V/Nk_B T$, at melting point was 13 to 15 as the electrolyte concentration was around 10^{-2}mole/liter. These values are close to the computed value 11.6 ($P_m V_o/Nk_B T.V/V_o=8.6\times1.35=11.6$, where V_o is the system volume at the state of the closest packing and the point of melting is $V/V_o=1.35$) by *Alder et al.*[34] for hard sphere system, hence indicating that the particles in the experiment of *Takano et al.* behave as a hard sphere system in sedimentation. At low electrolyte concentrations, the value of the reduced pressure was larger and in accord with the result of *Hoover* et al.[35] for soft core system. In table (1.4) values of the reduced pressure and volume

fraction $\Phi_m = \rho\pi a^3/6$ (where ρ, a are the number density and diameter of the particle respectively) are given for *Takano et al.* work together with those of *Alder et al.*.

4.3 Crystallization in Coulomb liquids:

Ionic crystals are the first example that comes to mind in relation to crystallization under *Coulombic* interactions. In an idealized picture, an ionic crystal is made up of positive and negative ions and the interaction between the different types of ions is the long range electrostatic term $\pm q^2/r$ (attraction between ions of opposite charge and repulsive between ions of same charge). The electrostatic interactions of these point like charges give rise to a net binding (*Madelung* energy), as each ion is preferentially surrounded by ions of opposite charge. In typical crystal, the *Madelung* energy is in fact close to the observed cohesive energy, which is required to disassemble the crystal into its consistuent ions.

The interaction U_{ij} between ions i and j at distance R is the sum of a short range core-core repulsion potential and a *Coulomb* potential, written as

$$U_{ij} = U^{core}(R) \pm U^{Coul}(R) \quad , \qquad (1.26)$$

where the positive sign is taken for the like charges and the negative sign for the unlike charges. It is clear that $U^{core}(R)$ describes the fact that each ion resists overlap with the electron distribution of neighbouring ions. In the absence of overlap forces, the crystal would

collapse.

From phenomenological point of view, the role of *Coulomb* interactions in the freezing of molten salts is demonstrated[36] by noticing that a critical values of a suitably defined coulombic coupling strength appears to be involved, at least for the alkali halides freezing at atmospheric pressure. The coupling parameter may be defined as

$$\Gamma = \frac{e^2/r_o}{k_B T} \quad , \qquad (1.27)$$

weher r_o is the interparticle spacing. Clearly, this parameter measures the ratio between the *Coulomb* energy and the thermal kinetic energy and the data show that freezing occurs at Γ=70.

However, the most marked similarity between colloidal crystals and other systems of charges that show crystalline order, would be found with metals and the (classical) *Wigner* crystal. In both cases the charges of one sign are localized on a crystal lattice and the charges with opposite sign are delocalized in a "neutralizing background". Within the idea of *Wigner* crystallization, *Fuchs*[37] calculated the *Madelung* energy for an f.c.c. and a b.c.c. lattice and found that the difference between *Coulomb* ground state energies is extremely small. Table (1.5)[35] shows different values of *Madelung* constant α_m for neutralized *Bravais* lattices and ionic crystal structures, in which the *Madelung* energy is defined as $-\alpha_m(Ze^2)/a$ where Z is the largest common factor of the ionic valences and a is the nearest neighbour distance.

5. Crystallization and Liquid gas transition under pure Coulombic forces.

For colloidal particles one needs not only the *Madelung* energy to discuss crystallization from energy considerations, but needs also to take into consideration the entropy of particle motions. The theory of melting and freezing has a long history. *Kirkwood* and *Monroe*[39] developed a theory of the liquid-solid transition which was based on the BBGKY hierarchy for inhomogenous systems and requires at least the knowledge of the pair potential V(r) and the homogenous pair distribution function g(r). *Ramakrishnan* and *Yusouff* (RY)[40] constructed a theory of freezing using the grand canonical ensemble, and *Haymet* and *O*xtoby[41], in the course of studying the structure of the crystal-liquid interface, recast the RY theory into the language of density functional theory and the direct correlation function c(r). In this theory the solid-phase density, which is a periodic function of position **r** in the crystal, is expanded in its *Fourier* components which allowed to vary so as to minimize the free energy, subject to the symmetry constraints of the crystal under investigation. The order parameters of the phase transition are the mean density $(\rho_{solid}-\rho_{liquid})/\rho_{liquid}$ and the *Fourier* components which are zero in the liquid, but take spontaneously finite values at freezing.

The classical plasma on an inert background is known from simulation work to crystallize in a b.c.c. lattice when its *Coulomb* coupling constant $\Gamma=e^2/r_s\epsilon k_B T$ equals approximately 180. Freezing occurs, of course, under purely repulsive *Coulomb* forces and the density is maintained at any chosen value by fixing the density of background. The density-wave theory of freezing, developed by RY for

classical liquid was analyzed in detail in relation to the crystallization of a classical plasma on a neutralizing background into a body-center cubic lattice[42]. It was pointed out that the equilibrium between solid and liquid at coexistence was maintained in this model system by an interfacial dipole layer. There still are difficulties in a full microscopic theory of the crystallization of the classical plasma, owing to a relevant role of non-linear (three-body) correlations. However, in relation to macroion solution one must keep into account the role of counterions (giving an "active background" through screening) and possibly also an active role of the solvent.

5.1 Debye-Hückel theory:

In the *Debye-Hückel* (D-H) approach one selects an arbitrary ion of charge Ze out of the assembly as a reference ion and considers the water molecules as a continous dielectric medium with dielectric constant ϵ_o, whereas the remaining ions of the assembly enter the analysis as an excess charge density $\rho_r(r)$. Thus the problem is reduced to a simple one, how to find the excess charge density $\rho_r(r)$ which varies with distance r from the reference ion. The electrolyte solution as a whole is electroneutral, i.e. the net charge density is zero.

One solves *Poisson's* equation for such system,

$$\frac{1}{r^2}\frac{d}{dr}\left(r^2\frac{d\phi(r)}{dr}\right) = -\frac{4\pi}{\epsilon_o}\left[\rho_r(r)-\sum_i n_{io}Z_i e\right] \quad , \qquad (1.28)$$

using the *Boltzmann* distribution law of classical statistical mechanics

$$n_i(r) = n_{io}\exp(-Z_i e\phi(r)/k_B T) \quad , \qquad (1.29)$$

for the number $n_i(r)$ of ions i per unit volume arround the chosen ion. Notice that

$$\rho_r(r) = \sum_i n_i(r) Z_i e \quad . \qquad (1.30)$$

An analytic solution is immediately found on the assumption that the electrostatic interactions are weak compared to the thermal energy, i.e.

$$Z_i e\phi(r) \ll kT$$

expanding the exponent in eq.(1.29) one finds that for a point-like ions the electrostatic potential is

$$\phi(r) = A\,\frac{e^{-\kappa r}}{r} \quad , \qquad (1.31)$$

where

$$A = \frac{Ze}{\epsilon_o} \quad , \qquad (1.32)$$

Ze being the charge on the chosen ion, and κ is the invers *D*ebye screening length givrn by

$$\kappa^2 = \frac{4\pi e^2}{\epsilon_o k_B T}\sum_i n_{io} Z_i^2 \quad . \qquad (1.33)$$

For a colloidal suspension of volume V with N particles (macroions) of charge -Ze and the equivalent number ZN of counterions of charge e, the free energy is the sum of the perfect gas contribution F_p and the free energy F_{el} of electrostatic interactions in the *Debye-Hückel* approximation[4]. Omitting terms that are irrelevant for phase transitions, we have

$$F_p = -k_B T(N \ln \frac{V}{N} + ZN \ln \frac{V}{ZN}) \quad , \qquad (1.34)$$

and

$$F_{el} = -\frac{1}{3} \frac{e^2}{\epsilon_o} \kappa \ (NZ^2+NZ)$$

$$= -\frac{1}{3} k_B T \ L_B \kappa \ (NZ^2+NZ) \quad , \qquad (1.35)$$

where $L_B = e^2/\epsilon_o k_B T$ with dimension of length (known as *Bjerrum* length). We can see from eq.'s (1.34) and (1.35) that the perfect-gas part $F_p \sim -\ln V$ decreases with increasing the volume V, which means that the system considered as a perfect gas has a tendency to explode. On the other hand the electrostatic part $F_{el} \propto -V^{-1/2}$ increases with increasing V. One can measure the relative importance of the two competing contribution by calculating of the pressure $P=-(\partial F/\partial V)_T$, i.e.

$$P = k_B T \frac{N+ZN}{V} - \frac{\sqrt{\pi}}{3} [L_B \frac{NZ^2+NZ}{V}]^{3/2} \quad , \qquad (1.36)$$

In the case where $Z \gg 1$ one gets

$$P \simeq k_B T \ Zn \ (1 - \frac{\sqrt{\pi}}{3} \sqrt{L_B^3 n \ Z^2}) \quad , \qquad (1.37)$$

where $n=N/V$ is the density of macroions. Hence one finds a critical density at which the bulk modulus $n(\partial P/\partial n)_T$ vanishes

$$n_{crit} = \frac{4}{\pi} (\frac{1}{B^3 Z^4})$$

By analogy with phase diagram for ordinary fluids (liquid-gas coexistence curves), the above result has been considered by various authors as an indication that the present model may undergo a phenomenon of condensation under pure *Coulomb* interactions. With

L_B=74A° and Z≈230 one finds $n_{crit} \simeq 10^{12}$ particle cm^{-3}. We shall return to this question in section (5.3) below after reviewing work on crystallization in an effective repulsive potential of the form of eq.(1.31).

5.2 Crystallization in the Yukawa potential:

A study of melting in aqueous suspension of polystyrene spheres was presented by *Shih et al.*[43,44], where their approach was based on the assumption that the intersphere interaction can be represented as screened *Coulomb*. At this level the presence of counterions enters only through the screening length and the role of the medium enters only through the static dielectric constant ϵ_o. The main calculation of *Shih et al.* considered also the question of the possibility of reentrant, by which they mean that the polystyrene sphere suspension first freezes and then remelt as the density of spheres is increased at constant temperature and PH. They found that if the interaction between the spheres is approximated by the *Debye-Huckel* potential that corresponds to point charges a reentrant melting does take plase, whereas if a size-corrected *Debye-Hückel* interaction is used as a more reliable description, the reentrant phenomenon disappears.

Consider a colloidal suspension of N particles, each of radius a, in volume V, at absolute temperature T. Each of the N particles has an effective charge of Z electronic charges. If the suspension is not too dense and the temperature is not too low, then the interaction between ions (macroions) can be treated within the *Debye-Hückel* approximation.

If the spheres are regarded as point-like then, as we have seen in section (5.1), the interaction takes the form

$$\phi(r) = \frac{Z^2 e^2}{\epsilon_o r} e^{-\kappa r} \quad . \qquad (1.38)$$

Following *J.O'M. Bockris*[45] an account for finite size of the particles can easily be introduced as follows. The linearized *Poisson-Boltzmann* equation for the electrical potential generated by a charged sphere in the system reads

$$\frac{1}{r^2} \frac{\partial}{\partial r} (r^2 \frac{\partial \phi(r)}{\partial r}) = \kappa^2 \phi(r) \quad , \qquad (1.39)$$

and its general solution is

$$\phi(r) = A \frac{e^{-\kappa r}}{r} \quad , \qquad (1.40)$$

where the physical requirement that $\phi(r) \longrightarrow 0$ as $r \longrightarrow \infty$ is satisfied. In evaluating the constant A in eq.(1.40), the point-like D-H approximation has been made. In order to take the size of the ions (macroions) into consideration, we recall that the charge dq in any particular shell of thickness dr at distance r from the origin of the ion is

$$dq = \rho_r 4\pi r^2 dr \quad , \qquad (1.41)$$

where ρ_r is the charge density obtained as

$$\rho_r = -\frac{\epsilon}{4\pi} [\frac{1}{r^2} \frac{\partial}{\partial r} (r^2 \frac{\partial \phi(r)}{\partial r})] = -\frac{\epsilon}{4\pi} \kappa^2 \phi(r) \quad , \qquad (1.42)$$

and as $\phi(r)$ is known from eq.(1.40) one obtains

$$\rho_r = -\frac{\epsilon}{4\pi} \kappa^2 A \frac{e^{-\kappa r}}{r} \quad . \qquad (1.43)$$

Thus, the charge dq is

$$dq = -\epsilon A\kappa^2(e^{-\kappa r} r\ dr) \quad , \qquad (1.44)$$

and the total charge in the ion cloud (q_{cloud}) must be equal to -Ze by electroneutrality. Hence for a sphere of radius a we have

$$q_{cloud} = -Ze = \int_a^\infty dq = -A\kappa^2\epsilon\int_a^\infty e^{-\kappa r} r\ dr \quad , \qquad (1.45)$$

clearly one is assuming that the ion cloud starts from the surface of the macroion. Eq.(1.45) yields

$$A = \frac{Ze}{\epsilon_o}\ \frac{e^{\kappa a}}{1+\kappa a} \quad . \qquad (1.46)$$

From this argument *Shih et al.*[43,44] considered the effective interaction between macroions to take the following form

$$\phi(r) = \frac{Z^2e^2}{\epsilon_o r}\left(\frac{e^{\kappa a}}{1+\kappa a}\right)^2 e^{-kr} \quad , \qquad (1.47)$$

such interaction takes into account the fact that part of the volume of the suspension is not available to the screening counterions, since it is occupied by the macroions.

To locate the coexistence line in the phase diagram, it was calculated by comparing the *Helmholtz* free energy of different phases (b.c.c.,f.c.c.,hcp and liquid) at the same temperature. The *Helmholtz* free energy per particle F takes the following form:

$$F = \frac{1}{2N}\left(\frac{e^{\kappa a}}{1+\kappa a}\right)^2 \sum_{i\neq j} \frac{Z^2e^2}{\epsilon_o} \left\langle \frac{1}{|r_i - r_j|}\ e^{-k|r_i - r_j|} \right\rangle + E_{kin} - TS \ , \qquad (1.48)$$

where E_{kin} and S are the kinetic energy and entropy per particle, < > denotes the thermal average over the canonical ensemble, and **r** is the position of particle i. Eq. (1.48) includes only terms of the free

energy which depend on the arrangement of particles. The *Einstein* oscillators and the hard sphere fluid were used as the reference systems for the solid and liquid, respectively[44]. The authors show that solid phases are stable at low salt concentrations: b.c.c. is preferred only at high charges and low densities while f.c.c. is dominant at higher densities. The solid phase melt upon addition of salt: b.c.c. may or may not transform to f.c.c. before melting, depending on the particle number densities $D=N/V$. Fig.(1.18) shows results in the D-ρ plane (where ρ is the salt concentration) at different values of Z, one can see that the colloidal suspension freezes when the particle number density is sufficiently high. The f.c.c. phase is formed in most of the high density region, whereas the b.c.c. phase is stable only in a very narrow region of lower densities. The density range of the f.c.c. phase shrinks as electrolytes are added to solution, and the b.c.c. phase completely disappears when the salt concentration is greater than about 2.5×10^{-8}M. Beside this, the addition of electrolyte will also make the crystalline phases become less favorable and eventually melt into liquid.

Defining the effective temperature as $\tilde{T}=k_BT/(Z^2e^2/\epsilon_o a_s)$ and measuring the screening strength in terms of the dimensionless parameter κa_s, where $a_s=(V/N)^{1/3}$ is the average nearest neighbour distance, the phase diagram can be plotted in the $\tilde{T}$-κa_s plane (fig.1.19). The liquid phase is stable at high $\tilde{T}$ and large κa_s (i.e. small Z and high salt concentration). At low $\tilde{T}$, b.c.c. phase is preferred at small κa_s, and the f.c.c. phase at large κa_s. Finally in fig.(1.20) they plot the density range of the three phases as a function of the particle charge Z at zero salt concentration. The

b.c.c. region becomes narrower and finally closes up when Z is decreased. It is also clear from this figure that a large charge can retain the crystalline phases to a low density.

5.3 Oscillatory screening:

In general, oscillatory screening phenomena should be expected when the *Debye* length $1/\kappa$ is in competition with another characteristic length of the system. In colloidal suspensions, one type of ions (macroions) is of large size a, which can compete with the *Debye* length. It was recognized by *Kirkwood*[46] that finite ion size could drastically alter the physics of electrolytic solutions at high ionic strength. In the case of point ions, the test charge is surrounded by a cloud of oppositly charged ions which effectively screen the test charge and neutralize it when viewed from distances much larger than the screening length. Increasing ionic strength simply decreases the screening length. If the ions have a finite radius, the density of ions in the screening cloud can not increase indefinitely, and at a critical ionic strength the ion cloud surrounding a test charge stratifies. At this point alternate layers of positive and negative charge form around the central ion. *Hastings*[47] applied *Kirkwood's* theory to solutions of macroions in the presence of counterions, and discussed the predictions of the theory in the context of experimental results.

Kirkwood's approach consists of considering the ions as impenetrable charge spheres which interact via the potential

$$V_{\alpha\beta}(r) = \infty \qquad r<a_{\alpha\beta}=R_\alpha+R_\beta$$

$$= \frac{Z_\alpha Z_\beta e^2}{\epsilon r} \qquad r>a_{\alpha\beta} \qquad , \qquad (1.49)$$

where R_α is the radius of an ion of type α and $Z_\alpha e$ is the charge on this ion. In this model he neglect the solvent-soluble interaction and assume that the ions are immersed in a medium of dielectric constant ϵ.

In the theory screening of the bare potential arises in the effective pair interaction between ion 1 and 2 of species α and β which is given by the integral equation

$$W_{\alpha\beta}(r_{12}) = \frac{Z_\alpha Z_\beta e^2}{\epsilon r_{12}} - \sum_\gamma \frac{n_\gamma Z_\gamma Z_\alpha e^2}{\epsilon k_B T} \int dr_3^3 \frac{W_{\beta\alpha}(r_{13})}{r_{13}} \theta(r_{13}-a_{\alpha\gamma})\theta(r_{23}-a_{\beta\gamma}) \qquad (1.50)$$

where n_γ is the concentration of the ionic species γ, and the θ functions in the integrand are to exclude the regions of particle overlap from the domain of integration. The pair correlation function for species α and β is given by

$$g_{\alpha\beta} = \exp[-W_{\alpha\beta}(r_{12})/k_B T] \qquad . \qquad (1.51)$$

By making the subsitution

$$W_{\alpha\beta}(r_{12}) = \frac{Z_\alpha Z_\beta e^2}{\epsilon r_{12}} \phi_{\alpha\beta}(r_{12}) \qquad , \qquad (1.52)$$

and carrying out the angular integration in eq.(1.50), one gets

$$\phi_{\alpha\beta}(r_{12}) = 1-\sum_\gamma \kappa_\gamma^2 \int_{a_{\beta\gamma}}^{\infty} dr' \; F_{\alpha\gamma}(r_{12},\gamma')\phi_{\beta\gamma}(r') \qquad , \qquad (1.53)$$

where

$$\kappa_\gamma^2 = \frac{4\pi n_\gamma Z_\gamma^2 e^2}{\epsilon k_B T} \qquad , \qquad (1.54)$$

is the contribution to the screening from the ionic species γ, and the *Kernel* $F_{\alpha\gamma}$ is given by

$$F_{\alpha\gamma}(r,r') = r \qquad , \quad a_{\alpha\beta}<r<r'-a_{\alpha\gamma}$$

$$= \frac{1}{2}(r+r'-a_{\alpha\gamma}) \qquad , \quad r'-a_{\alpha\gamma}<r<r'+a_{\alpha\gamma}$$

$$= r' \qquad , \quad r'+a_{\alpha\gamma}<r<\infty \qquad . \qquad (1.55)$$

Equation (1.53) may be solved using *Fourier* inversion techniques, provided that one imposes the condition $\phi_{\alpha\beta}(r)=\phi_{\beta\alpha}(r)$. The solution takes the form

$$\phi_{\alpha\beta}(r) = \sum_j A^j_{\alpha\beta} e^{ik_j r} \qquad , \qquad (1.56)$$

where k_j are the roots of a secular determinant

$$\mathrm{Det}[k^2 1+M(k)] = 0 \qquad , \qquad (1.57)$$

and the elements of the matrix M(k) are given by

$$M_{\alpha\gamma}(k) = \kappa^2_\gamma \cos(ka_{\alpha\gamma}) \qquad . \qquad (1.58)$$

This solution is valid in the region $r>2a_{max}$, where a_{max} is the diameter of the largest of ionic species, since it is the longe range behaviour of the potential that is important. In this region solutions of eq.(1.57) with a positive imaginary part are acceptable since the potential must be regular as $r \longrightarrow \infty$.

For binary solutions of ions of equal diameter a, eq.(1.57) reduces to the transcendental equation

$$k^2+\kappa^2\cos(ka) = 0 \qquad . \qquad (1.59)$$

For values of $\kappa a<1.03$ there are two pure imaginary roots and a pair of complex roots of the form $k=\pm k_1+ik_2$ (the complex conjugates of these roots also satisfies eq.(1.59), but are irrelevant due to their negative imaginary part). For values of $\kappa a\ll 1$ three of four roots have large imaginary parts and therefore give a negative contribution to the potential, while the remaining root is the *Debye-Hückel* solution $k=i\kappa$. As κa increases the pure imaginary roots approach each other and merge at $\kappa a=1.03$. In the range $1.03<\kappa a<2.79$ all solutions of eq.(1.59) are complex and the potential in this region is oscillatory and damped. For values of $\kappa a>2.97$ eq.(1.59) admits two purely real solutions, which give rise to an undamped oscillatory potential. Such solutions cannot satisfy the original integral (eq.1.53) since the integral over an undamped potential is undefined. Hence $\kappa a=2.79$ is the critical value which signals a transition to a state in which the potential is long ranged and oscillatory, with alternate layers of positive and negative charge forming around a given ion. At the critical value of κa eq.(1.59) has real solution with $\kappa a=2.46$. Therefore the wavelength of oscillation in the potential at critical point is $\lambda_c=2\pi a/2.46=2.55a$.

Hasting[47] assumed that the new state acquired by the system is a crystal with lattice constant roughly equal to λ_c and obtained an estimate for the unknown effective charge. From eq.(1.54) at the critical point

$$\kappa a = 2.79 = \left(\frac{4\pi n Z^2 e^2}{\epsilon k_B T}\right)^{1/2} a \qquad , \qquad (1.60)$$

where n is the concentration of binary salt, $n=1/(4/3\pi r_o^3)$, where r_o is

the average ion separation. At T=300°K and with $\epsilon \simeq 80$ one find from eq.(1.60)

$$2.79 = \frac{a}{r_o} Z(\frac{21}{r_o} A^o)^{1/2} \quad , \qquad (1.61)$$

Hasting took r_o for a binary salt to be half the wavelength of the oscillatory potential and obtained

$$Z_c = 0.88\sqrt{a} \qquad (a \text{ in } A^o,\ T=300^oK) \quad , \qquad (1.62)$$

However, the same argument applied to a molten salt like NaCl would lead one to predict crystallization at a value of the effective ionic valence much less than unity (or, more appropriately, at an excessively high temperature). The identification of *Kirkwood's* critical point (for insurgence of oscillatory screening) with crystallization appears to be false. These situation will be clarified by the discussion in the next section.

5.4 Liquid-gas coexistence in systems of charged hard spheres:

The classical fluid of point charges ambedded in a uniform background (one-component plasma, or OCP) is often taken as a prototype model for understanding the behaviour of real charge fluids. Computer simulation work[48,49] on its thermodynamic properties shows that the "compressibility" of the OCP becomes negative with increasing plasma parameter Γ. At approximately the same value of Γ, oscillations are found to appear in the charge-charge radial distribution function $g_q(r)$.

A negative value of the compressibility is commonly associated with a mechanical instability of the system[50]. In the OCP, instead, one is observing a change in the character of the screening, from exponential to oscillatory, as Γ increases, while mechanical stability of the model is preserved through the boundary condition imposed on the simulation runs.

The next model in order of complexity is a fluid of two types of equi-sized, charged hard spheres with charges +e and -e (restricted primitive model, or RPM). This model possesses a true compressibility in combination with classical screening properties. *Stell et al.*[51] gave evidence for a liquid-gas coexistence curve and critical point in the RPM, using various representation of the equation of state. The result are shown in fig.(1.21) while different approximate equations of state lead to qualitatively different results, they all agree in showing the existence of a critical point. In addition, there is a change in character of the screening from monotonic to oscillatory as one goes from low-density ("gas-like" or "plasma-like") to high-density ("liquid-like") states.

A similar calculation for the RPM, carried out in the MSA, is shown in fig.(1.22)[52]. The isotherms have the classical *van der Waals* shape with a liquid-gas critical point. Phase separation is again found below critical pressure. The two phases are characterized by values of the inverse screening length (κ_s) which are imaginary for the high density (liquid) phase and real for the low density (ionized gas) phase. These correspond, respectively, to an oscillatory and exponential asymptotic screening behaviour. The critical point is between the locus of points in the pressure density plane where κ_s^2

changes sign and the locus of points where oscillations in $g_q(r)$ appear. The equation of state is given analytically by the MSA (which we will discuss in some detail in chapter 3) as

$$P = 2nk_BT \frac{1+\eta+\eta^2}{(1-\eta)^3} + \frac{k_BT}{4\pi\sigma^3} [x+x(1+2x)^{1/2} - \frac{2}{3}(1-2x)^{3/2} + \frac{2}{3}] \quad , \tag{1.63}$$

where n is the number of ion pair per unit volume, $\eta = \frac{1}{3}\pi n\sigma^3$ is the packing fraction, σ is the hard sphere diameter, and $x=\kappa_{DH}\sigma$ with κ_{DH} the *Debye-Huckel* inverse screening length.

An analytic expression for κ_s^2 can be obtained from the low κ expansion of the charge-charge structure factore $S_{qq}(k)$ defined as

$$S_{qq}(k) = \frac{1}{2} [S_{++}(k) + S_{--}(k) - 2S_{+-}(k)] \quad , \tag{1.64}$$

by using the fluctuation-dissipation theorem to relate $S_{qq}(k)$ to the response function $\chi_{qq}(k,0)$

$$S_{qq}(k) = -\frac{k_BT}{2n} \chi_{qq}(k,0) \quad , \tag{1.65}$$

and from the long-wavelength expression[53] for the static charge responce function

$$\lim_{k\longrightarrow 0} \chi_{qq}(k,0) = -\frac{\epsilon_\infty k^2}{4\pi e^2} (1 + \frac{k^2}{\kappa_s^2}) \quad , \tag{1.66}$$

after compairing the expression (1.64) and eq.(1.66). The result of this lengthy calculation is

$$(\kappa_s\sigma)^2 = x^2[\frac{1}{2} - \frac{1}{3}x - \frac{1}{12}x^2 - \frac{1}{6}x(1+2x)^{1/2} + \frac{1}{2}(1+2x)^{1/2}]^{-1} \tag{1.67}$$

with the limiting values $\kappa_s=\kappa_{DH}$ for $x\longrightarrow 0$ and $\kappa_s^2=-12/\sigma^2$ for $x\longrightarrow\infty$.

Finally, in relation to highly asymmetric polyelectrolytes, structural and equilibrium properties of a two component liquid of

charged hard spheres with very different charges and sizes have been studied recently in the hypernetted chain approximation (HNC) by *Belloni*[54]. As the concentration is decreased the osmotic compressibility increases and seems to diverge at a fixed (sufficiently low) temperature (see fig.1.23). The cut-off concentration is a point of the so-called spinodal line which is the frontier of an unstable region. Inside this region, negative compressibility leads to spinodal decomposition, i.e. phase separation. The spinodal line and the critical point were obtained for different charge dissymetries. In fig.(1.23) the normalized osmotic compressibility $\chi/\chi_o=k_BT(\partial\rho/\partial\pi)_T$ is plotted for $|Z_1/Z_2|=20$ versus the volume fraction $\Phi=\frac{\pi}{6}\rho_p\sigma_p^3$ at different values of the reduced temperature $T^*=a\epsilon k_BT/e^2$, where $a=\sigma_p/2$ is the polyion radius, and ρ_p is the number density of the polyions.

The "phase diagram" T^* vs Φ is given in fig.(1.24), showing different curves at constant osmotic compressibility. The special curve $\chi=+\infty$ which defines the spinodal line is obtained by extrapolation. In the infinite-dilution limit the compressibility differs from the ideal part by a positive term propotional to the square root of the concentration as given by *Debye-Hückel* low. Thus χ/χ_o increases rapidly from 1 at low concentration and diverges rapidly for $T^*<T^*_{crit}$ (see the begining of curve e fig.1.23). As a consequence, the rare phase is very dilute and occupies a very narrow part of the phase diagram (fig.1.24). We will discuss the liquid-gas transition in this type of model using the MSA in chapter 3 and comment on the differences between our work and *Belloni's* work.

5.5 Summary and conclusion:

Throughout this chapter, we have briefly reviewed colloidal suspensions, the various types of particle-particle interactions and the crystallization of colloidal particles. In the last section we have focussed on crystallization under pure *Coulomb* forces and or liquid-gas coexistece in systems of charged hard spheres.

From what we have seen we should like to stress the main points that we are going to deal with in the following chapters. First, it is clear from experimental work of *Ise et al.* on colloidal suspensions to measure the intermolecular ordering distance $2D_{exp}$ (discussed in section 2.3.3.), that "condensation" occurs in such systems, in the sense that the dense phase has density higher than allowed by the container volume. Hence there are effective attractive forces in these systems, which are ignored in models involving purely repulsive forces (i.e. the *Yukawa potential*). Secondly, from the work of *Belloni*[50], it is clear that "condensation" occurs in a simple model having a gas-to-liquid transition under pure *Coulomb* forces, and this again presupposes the existence of effective attractive forces.

In chapter 2 we will elaborate on a theoretical model suggested by *Sogami*[55]. We shall examine the equation of effective macroion-macroion potentials within linear response theory and examine the sensitivity of the results to the nature of the short range macroion-macroion interactions using the *Poisson-Boltzmann* approximation. Within this scheme one always finds an effective ion-ion repulsion of the *Yukawa* type as long as one looks at the *Helmholtz* free energy to define this effective interaction, and the only quation that

we shall be able to discuss will be the strength of this repulsion (the constan A discussed in section 5.2).

In chapter 3 we are instead concerned with constructing a liquid-gas coexistence curve for strongly asymmetric charge hard spheres using the MSA approximation. We shall aim at comparing our results with those predicted for the spinodal line by *Belloni*[54], giving in addition the "liquid-gas" equilibrium coexistence curve.

$N(cm^{-3})$	a_o(micron)	a_b(micron)	a_f(micron)
2×10^{13}	0.46	0.54±0.05	0.55±0.06
1×10^{13}	0.58	0.56±0.06	0.68±0.07
6.7×10^{12}	0.67	0.61±0.06	
5×10^{12}	0.74	0.70±0.08	
2×10^{12}	1.00	0.77±0.08	

Table 1.1[22]: Lattice constant as a function of latex sphere density N. a_o is the lattice constant for a b.c.c. lattice, calculated from the sphere density, using the relation $a_o=(2/N)^{1/3}$. a_b is the measured lattice constant for the b.c.c. lattice. a_f is the measured lattice constant for the f.c.c. lattice.

Expt.	M_w	Conc(9/ml)	S_m^a(A°-1)	$2D^b_{exp}$(A°)	$2D^c_o$ (A°)	Temp.(C°)
1	74000	0.01	0.040	157	231	25
2	74000	0.02	0.052	122	183	25
3	74000	0.04	0.073	87	145	25
4	74000	0.08	0.096	65	115	25
5	74000	0.16	0.134	47	92	25

Table 1.2[23]: Smale angle X-ray scatering data of *sodium polystyrene sulfonates* in aqueous solutions.

M_w= molecular weight os sample.

S_m^a= Scattering vector at the peak.

$2D^b_{exp}$ = Intermacroion distance obtained from S_m on the assumption that the *Bragg* equation holds.

$2D_o$= Intermacroion distance calculated for a simple cubic distribution.

volume fraction 100Φ	a_k(Å)	a_{Ds}(A°)	structure
0.6	7118±07	7248±20	b.c.c.
0.8	6705±30	6759±30	b.c.c.
1.0	6025±100	6283±40	b.c.c.
2.0	4939±60	4875±80	b.c.c.
3.0	5542±50	5552±10	f.c.c.
4.0	4965±100		f.c.c.
6.0	4344±70		f.c.c.
8.0	4141±30		f.c.c.
9.8	4061±80		f.c.c.

Table 1.3[24]: Crystal structures and lattice constant a_k determined by the *Kossel* rings, compared with the lattice constant a_{Ds} determined by *Debye-Scherrer* rings.

	Takano et al. values			Hard sphere values *Alder et al.*
Mole/L	10^{-2}	10^{-3}	10^{-4}	
$P^*=P_mV/NkT$	15	49	230	11.6
$=P_mV_o/NKT\times V/V_o$				
Φ	0.48	0.40	0.13	0.55
electrolyte KOH and T=307°K, Diameter=5630A°				
P^*	13	14	26	11.6
Φ	0.49	0.33	——	0.55
electrolyte KCl and T=293°K, Diameter=5000A°				

Table 1.4 Results of *Takano et al.* experiments together with the data of *Alder et al.*.For the reduced pressure P^* and the volume fraction Φ.

Structure	*Madelung* constant	
Neutralized s.c.lattice	1.41865	(0.88008)
Neutralized f.c.c.lattice	1.62099	(0.89587)
Neutralized b.c.c.lattice	1.57583	(0.8953)
Sodium Chloride (NaCl)	1.74756	
Cesium Chloride (CsCl)	1.76267	
Zincblende (ZnS)	1.63805	
Wurtzite (ZnS)	1.64132	
Fluorite (CaF_2)	5.03878	

Table 1.5: *Madelung* constant α_m for neutralized *Bravais* lattices and ionic crystal structures, refered to the first neighbour distance (first column) values in parantheses for the three *Bravais* lattices are refered to the distance $a=(4\pi n/3)^{-1/3}$ where n is the number density[38].

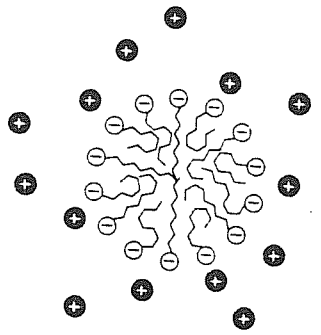

Fig.1.1: Schematic representation of a spherical or cylindrical micelle.

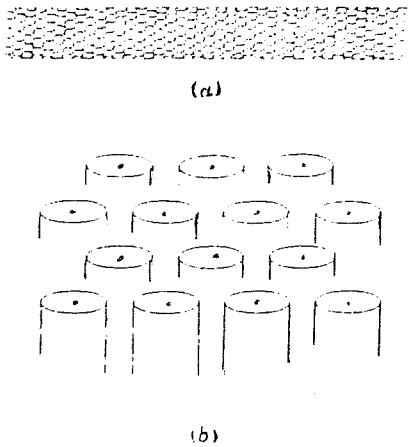

Fig.1.2.: Tobacco mosaic virus: (a) architecture: each shell is built of huge number of identical copies of one protein macromolecules. Globaly TMV is rod-shaped. 150-170A° in diameter and about 3000A° length. (b) Two-dimensional crystalline order.

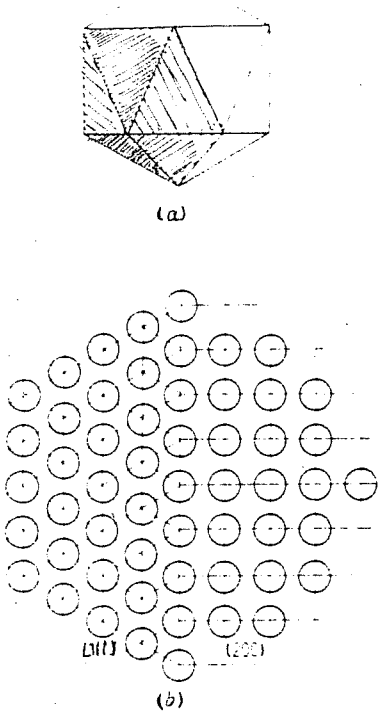

Fig.1.3.: Tipula virus: this larger insect virus has a protein shell, the approximate diameter of the whole virus is about 1300A° (a) an architecture design. (b) triangular and square arrays compatible with f.c.c. close packed structure observed by light microscope.

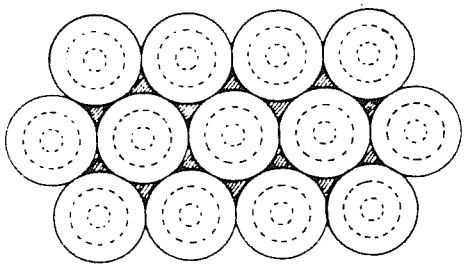

Fig.1.4.: Opal structure, tiny spherical silica particles cemented together, with voids filled with strongly hydrated form of amorphous silica.

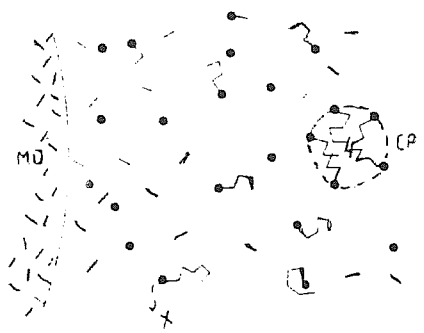

Fig.1.5.: Emulsion polymerization reaction. Monomer droplets (MD), insoluble in water. Initiator ● is already soluble in water. The reaction starts by forming oligomers. As they are large enough, a strong tendency towards segregation results in formation of colloidal particles. [surfactant molecules have been omitted from the drawing].

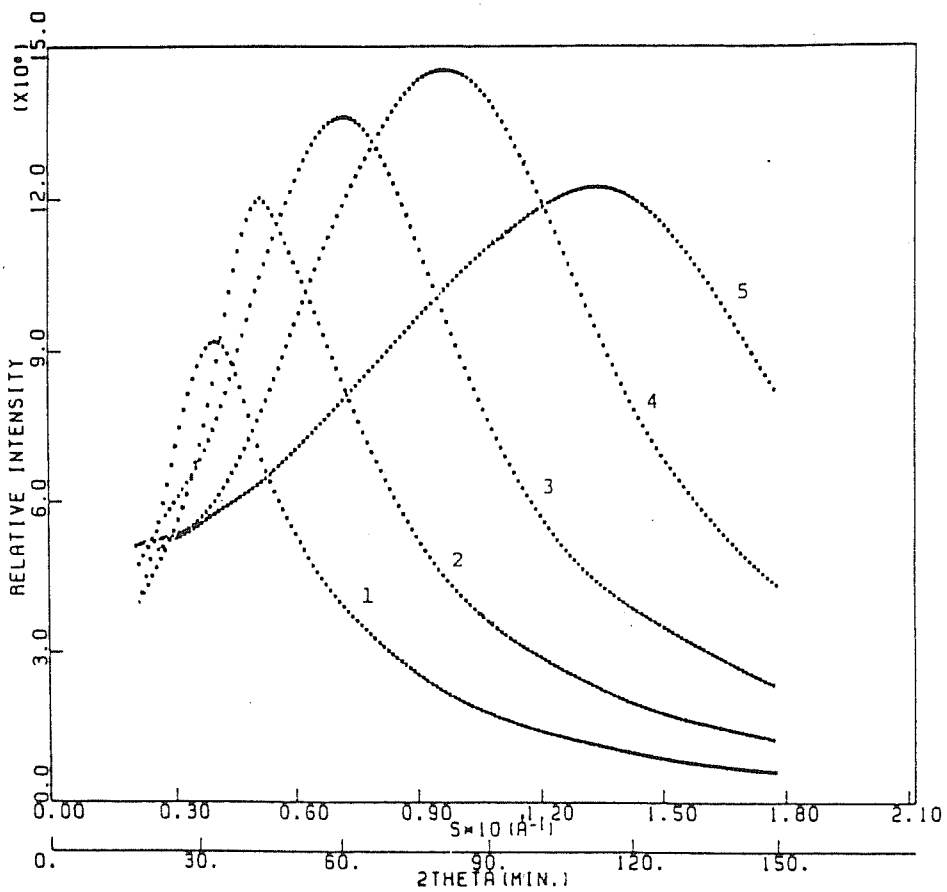

Fig.1.6.:Concentration dependence of scattering curves of NaPSS. M_w=74000, polymer concentration; curve 1:0.01 g/ml, 2:0.01 g/ml, 3:0.04 g/ml, 4:0.08 g/ml, 5:0.16 g/ml.

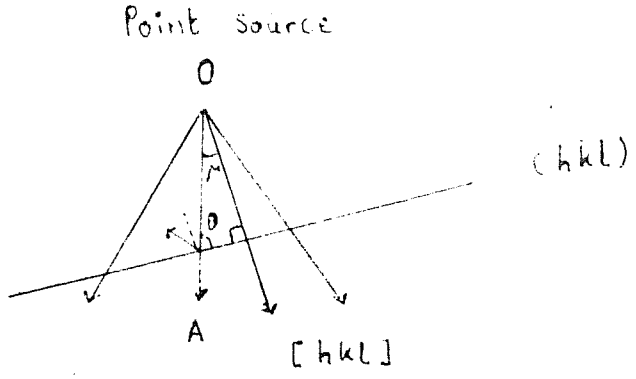

Fig.1.7.: Different rays from a point source forming a *Kossel* cone from ray OA.

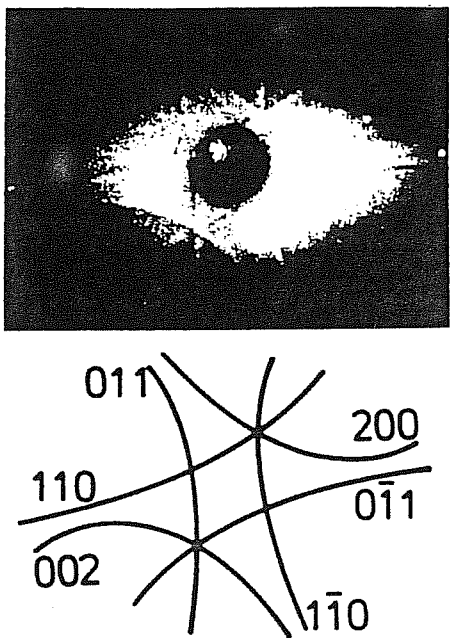

Fig.1.8.: Backward *Kossel* images with dark and bright fine structure from a colloidal crystal in polystyrene latex solution (1.5 vol%). The indices of the *Kossel* rings show that the crystal structure is b.c.c. and the incident direction of the laser beam is [101].

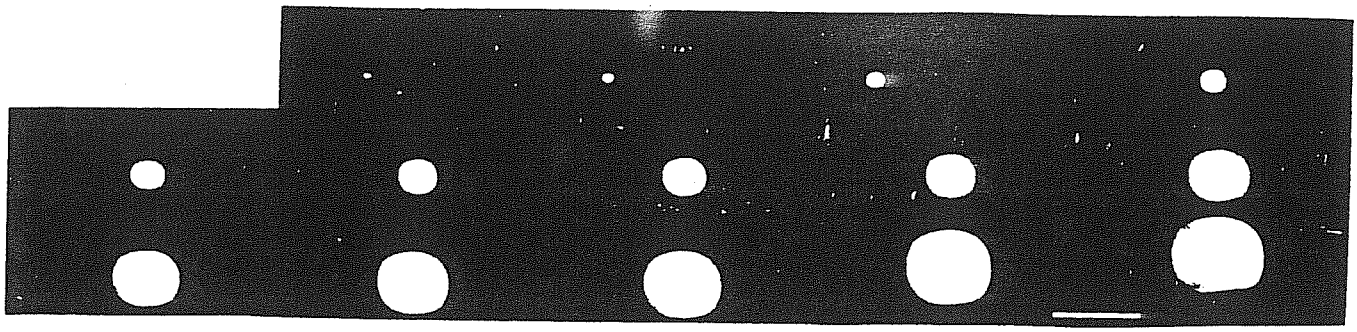

Fig.1.9.: A single b.c.c. colloidal crystal growing in a metastable liquid phase. Two seconds separate each frame and the fit frame occurs eight seconds after the cessation of rocking. The bar in the lower right-hand corner corresponds to a length of mm. The flattening of the bottom edge of the crystal in the last frame correspond not to the formation of a facet, but rather is the limit of growth in this direction as it has intersected with another crystal domain not in the *Bragg* condition. The crystal will continue to grow in the other directions until similar intersections occur.

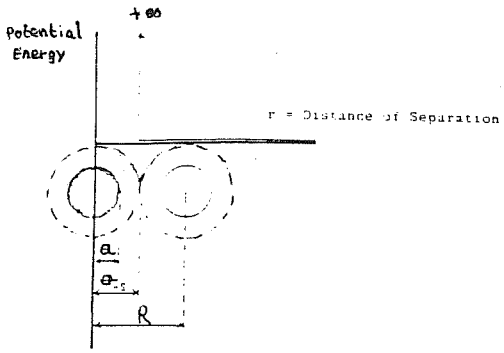

Fig.1.10.: Hard sphere interaction, a≡actual radius, a_{Hs}≡hard sphere radius, R≡ separation between particles.

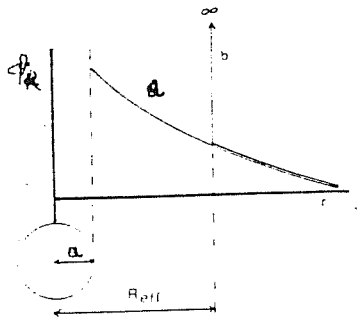

Fig.1.11.: Schematic plot of (a) ϕ_R. (b) hard sphere potential with soft tail.

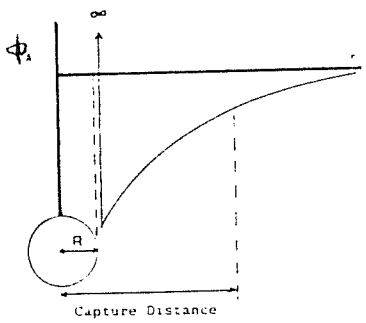

Fig.1.12.: Schematic plot of the attractive *van der Waals* interaction, concidered with a strong repulsion ($a \approx a_{eff}$).

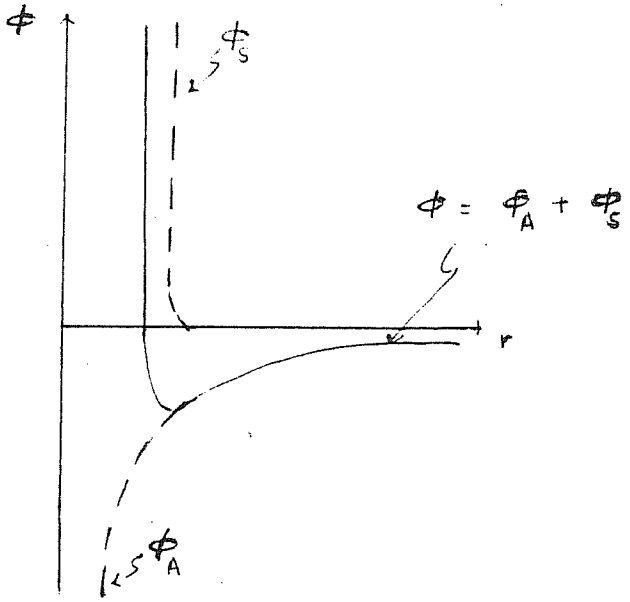

Fig.1.13.: Schematic plot of the total interaction energy; ϕ_A is the *van der Waals* potential, ϕ_s the steric repulsion potential.

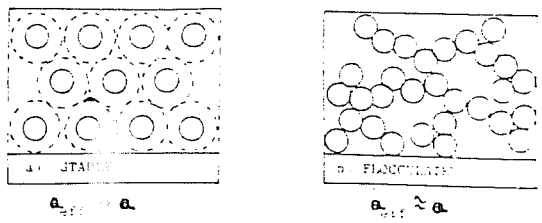

Fig.1.14.: Schematic plot of particle arrangement in a) stable system (ordered phase), b) flocculated system (disordered phase).—— particle radius a, ---- a_{eff}.

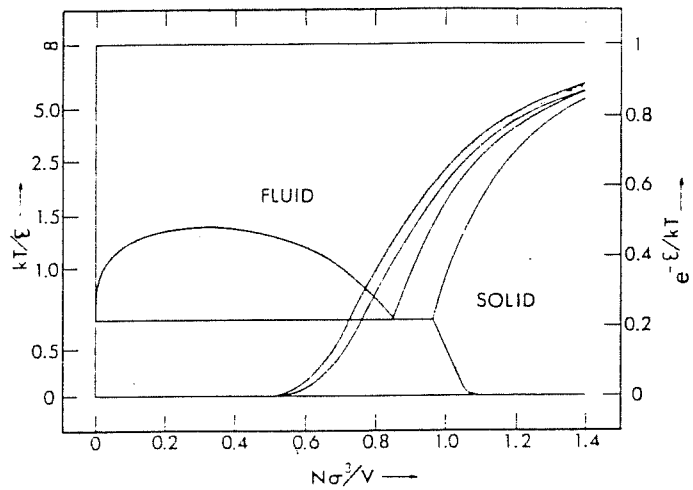

Fig.1.15.: The *Lennard-Jones* phase diagram, as determined at *Orsay* and *Los Alamos*. Superimposed on this diagram is the soft-sphere phase diagram resulting when only repulsive forces are used. The fluid-solid two-phase region for the soft-sphere potential is lightly shaded.

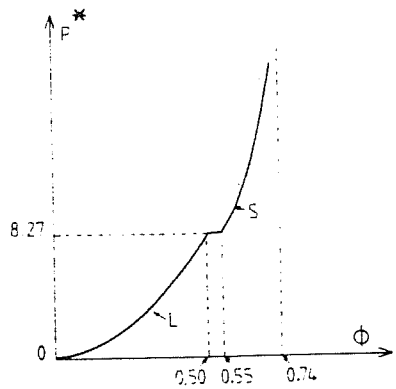

Fig.1.16.: Reduced pressure P^* as a function of volume fraction Φ in hard sphere model. Melting and crystallization occur at $P^*=8.27$. The corresponding volume fraction are $\Phi_s \simeq 0.55$ and $\Phi_l \simeq 0.50$.

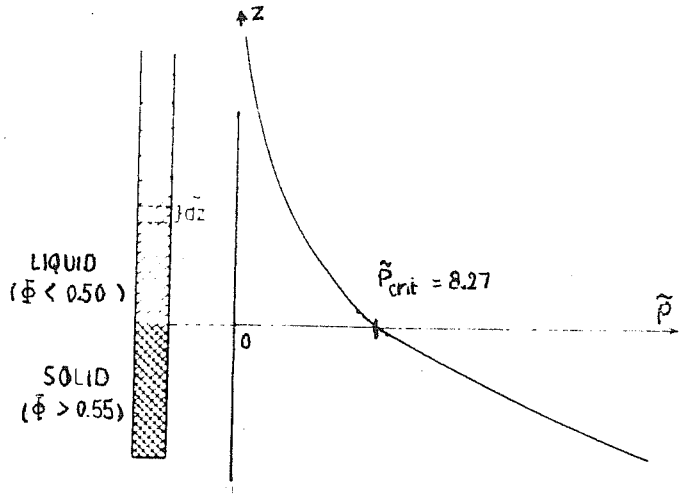

Fig.1.17.: The column of colloidal suspension is under gravitational forces effect. The pressure $\tilde{P}$ decreases with $\tilde{z}$ and at $\tilde{P}_{crit}$, $\tilde{z}\approx 0$, the density shows a discontinuity and a phase transition is located.

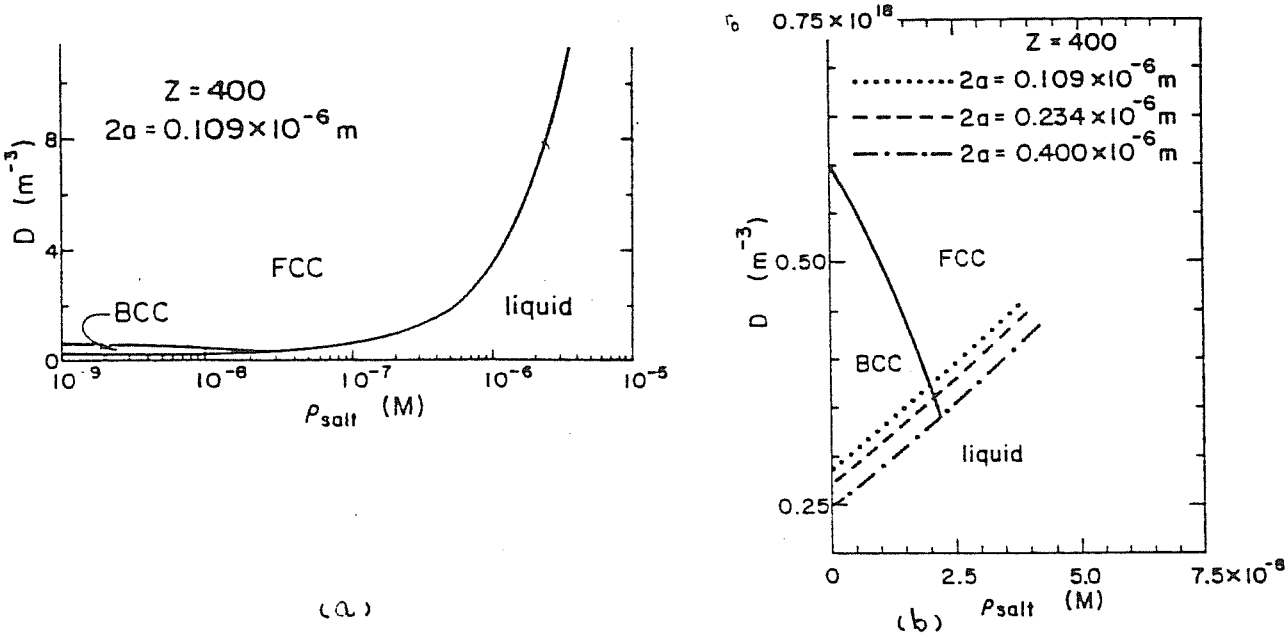

Fig.1.18.: D-ρ_{salt} phase diagram where D is the particle number and ρ_{salt} is the added salt concentration in molar units; (a) for a particle diameter $2a=0.109\times10^{-6}$m and charge Z=400; (b) in a different scale for Z=400 and $2a=0.109\times10^{-6}$, 0.234×10^{-6}, 0.400×10^{-6}m. The bcc-fcc phase boundaries are the same for the three cases while the liguid-solid phase boundaries are pushed to lower densities as particle size is increased.

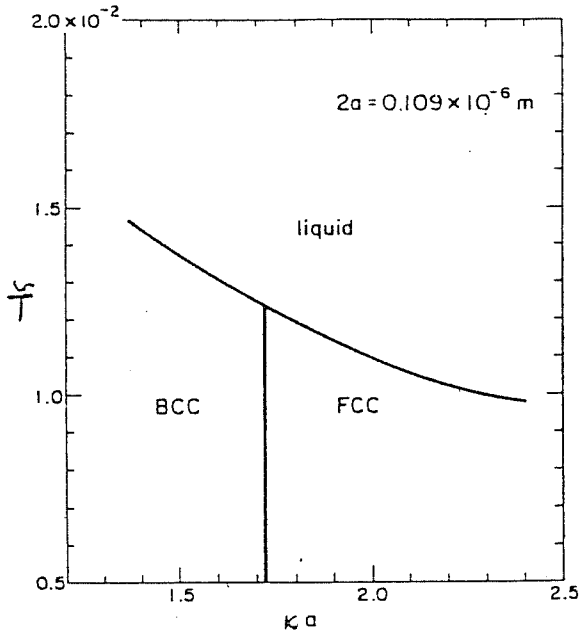

Fig.1.19.: The $\tilde{T}$-κa phase diagram for particles with diameter $2a=0.109\times10^{-6}$m. Where $\tilde{T}$,κ and a as defined in the text.

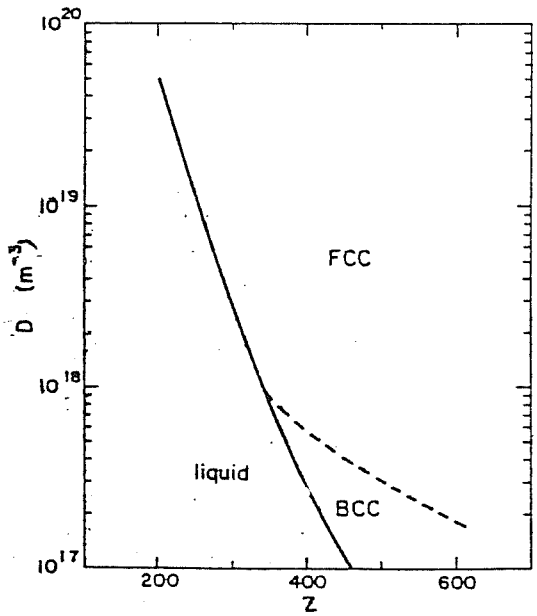

Fig.1.20.: The D-Z phase diagram for particles with diameter $2a=0.109\times10^{-6}$m and at zero salt concentration. bcc phase appears only when the charge Z is high and the particle number density D is low.

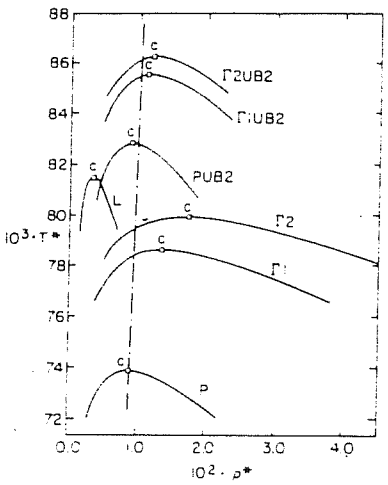

Fig.1.21.: Liquid-gas coexistence curves in the neighborhood of the critical point for the restricted primitive model in the various approximations. The straight line is the locus of points marking the onset of long-range charge-density oscillations in the lowest-order gamma-order approximation.

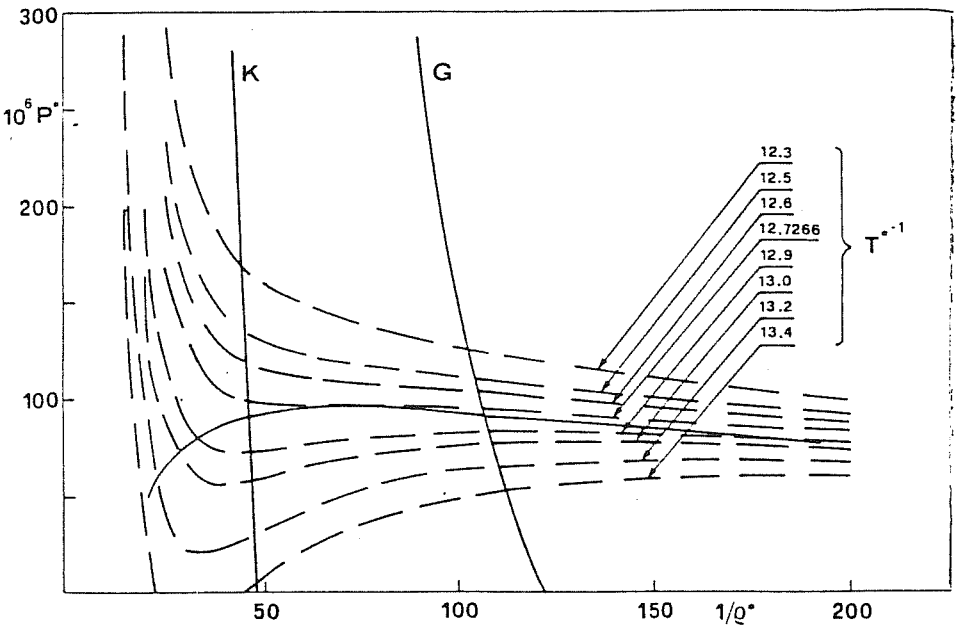

Fig.1.22.: Isotherms (broken lines) and coexistence curve (full line) of the model. Curves K and G give, respectively, the locus points where κ_s^2 changes sign and the locus of points where oscillation in $g_q(r)$ appear.

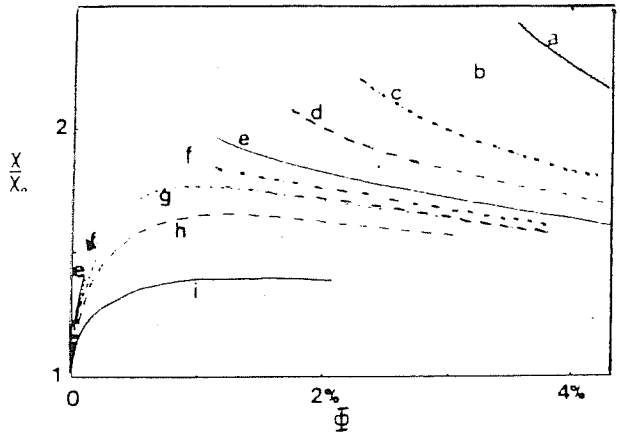

Fig.1.23.: Normalized compressibility vs volume fraction at different temperatures for Z=20. Curve a, $T^*=a/L_B=3.27$; curve b, 3.50; curve c, 3.73; curve d,3.97; curve e, 4.20; curve f, 4.32; curve g, 4.43; curve h, 4.67; curve i, 5.83.

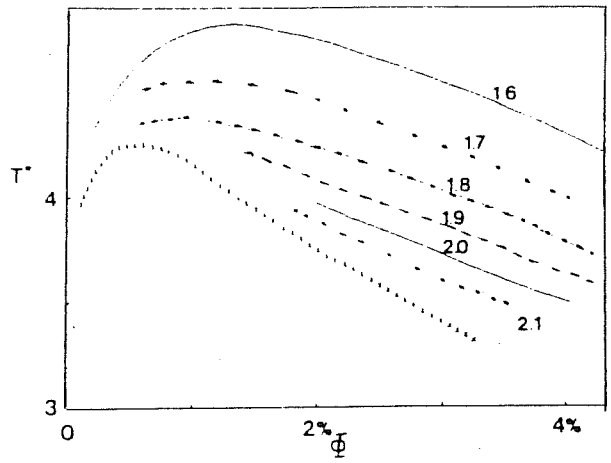

Fig.1.24.: Phase diagram T^* vs Φ for z=20. The different curves correspond to different values of the normalized compressibility. The last curve (crosses) represents the spinodal line.

CHAPTER II

EFFECTIVE ION-ION POTENTIAL IN POLYELECTROLYTE SOLUTIONS FROM LINEAR RESPONSE THEORY

1. Introduction:

It is the aim of much theoretical work to establish an expression for the effective pair interaction $v^{eff}(r)$ between macroions in a colloidal suspension. The most widely known and used expression is the DLVO potential[48], given most simply by

$$\beta v^{eff}(r) = +\infty \qquad r<\sigma_o \qquad (2.1a)$$

$$= \frac{Z_o^2/L_B}{(1+\kappa a)^2}\,\frac{e^{-\kappa(r-2a)}}{r} \qquad r>\sigma_o \quad , \qquad (2.1b)$$

where the index o represents the polyion, $a=\sigma_o/2$ is the polyion radius, $\kappa=(4\pi L_B\sum_i\rho_i Z_i^2)$ is the ionic inverse screening length due to the small ions, and $L_B=e^2/\epsilon k_B T$ is the *Bjerrum* length. This expression was already given in eq.(1.47),where the derivative of the "amplitude factor" $e^{2\kappa a}/(1+\kappa a)^2$ was reported.

This effective potential has been determined by using the *Debye-Hückel* equation for the small ions arround a colloidal particle. Thus within the DLVO there are three approximation:

(i) infinite dilution limit ($\rho_o \longrightarrow 0$).

(ii) point-like counterions.

(iii) weak polyion-ion interaction.

At the level of great simplification at which these systems can be treated theoretically, one should still try to determine the effective macroion-macroion potential by starting from the primitive model (PM)[54] for the solution as a mixture of charged hard spheres immersed in a continuous solvent of dielectric constant ϵ. Thus the "bare" pair potentials $v_{ij}(r)$, between ions i and j are

$$\beta v_{ij}(r) = +\infty \qquad r<\sigma_{ij}=(\sigma_i+\sigma_j)/2 \qquad (2.2a)$$

$$= \frac{Z_i Z_j L_B}{r} \qquad r>\sigma_{ij} \quad . \qquad (2.2b)$$

This model can be treated in its own right (as we shall do in chapter 3), in which the small ions would be treated on the same footing as the macroparticles. Of course, when this model is applied to real system, some questions arise, for example: what is the true significance of the hard-sphere size σ, or a charge Z for a micelle?. This is an important point which we will not discuss in detail but only comment upon by the end of this chapter (section 3).

In section 2 of this chapter, we will give a short description of a theoretical model suggested by *Sogami*[55,56]. Firstly, they removed the assumption of hard cores (eq.2.2a) for macroion-microion interactions, taking $\beta v_{12}(r)$ as negative constant inside the macroion "core". The electrostatic interactions were next treated by solving a generalized *Poisson-Boltzmann* equation with the linearization approximation. Thermodynamic properties were calculated, i.e. the

Helmholtz and *Gibbs* free energies for a general distribution of the macroions in space. Aside from an additive constant, these functions are sums of two-body macroion-macroion terms, which are identified with effective potentials. It was claimed that, while consideration of the *Helmholtz* free energy leads to purely repulsive effective interactions between macroions, consideration of the *Gibbs* free energy yields an effective attractive well at large distances. Thus, without any consideration of *van der Waals* attractions, their model can yield condensed phases for macroions (in the sense discussed in section 5.5 of chapter 1).

In section 3 we shall consider in somewhat greater generality the problem of the effective interactions between polyions, still assuming a soft core for the polyions and using a framework of linear response theory. Our main focus will be on the *Helmholtz* free energy and how different assumptions on the soft core affected the strength of the effective *Yukawa* repulsion between macroions once the *Poisson-Boltzmann* (or *Debye-Hückel*) approximation is made.

Finally, in section 4 we shall consider the transition from *Helmholtz* to *Gibbs* free energy. We shall see that, if one adopts the route followed by *Sogami*, then one finds similar predictions on condensation. However, we shall record at this point a recent critique of *Sogami's* work by *Ovebeek*[57], claiming that in fact there is exact cancellation between microions and solvent on the contribution given by *Coulomb* interaction to the difference between *Gibbs* and *Helmholtz* free energy. This will open the way for our work in chapter 3, where we shall attempt an approach to condensation which transcends the notion

of effective macroion-macroion interactions on a model system where the solvent is, however, still restricted to the purely passive role of a uniform dielectric medium.

2. Theoretical model for effective macroion interactions in colloidal supensions:

The model of *Sogami*[55] postulates the following:

(i) Macroions with uniform spherical shape of radius a carry an equal amount of electric charges Ze (Z<0) distributed uniformly on the surface.

(ii) The motion of the macroion particle is assumed to be addiabatically cut off from that of ions. The configuration of particles in suspension is determined so as to minimize the thermodynamic potential of the system which is derived by applying the adiabatic approximation[58] and expressed in terms of particle coordinates.

(iii) The particles and the ions are so dilute in suspension that the electric energy $z_i e\phi(r)$ of an ion with valence z_i is much smaller than the thermal energy $k_B T$, and consequently the number density $n_i(r)$ of the ions of type i is determined by the linearized form of the *Boltzmann* distribution, i.e.

$$n_i(r) = n_{io}[1-(z_i e/k_B T)\phi(r)] \quad , \qquad (2.3)$$

where n_{io} is the average number of ions of type i per unit volume.

(iv) The effect of water as medium arises only through the dielectric constant ϵ.

The electric potential $\phi(r)$ in the suspension satisfies the *Poisson-Boltzmann* equation, and the *Helmholtz* free energy F, is calculated from the total electrostatic energy of the system as a function of particle coordinates R_m. Then F is written as

$$F = F'+F^{el} = F'+E_{self}+\sum_n V_n^F +1/2 \sum_{m\neq n} U_{mn}^F \quad , \qquad (2.4)$$

where F′ is the energy with all the particles and small ions discharged and F^{el} is due to the charging process. For spherical particles with radius a

$$E_{self} = \sum_n \frac{(Ze)^2}{2\epsilon a}$$

$$V_n^F = \frac{(Z_n e)^2}{4\epsilon\kappa a_n^2} (1-e^{-2\kappa a_n} -2\kappa a_n)$$

and

$$U_{mn}^F = \frac{(Ze)^2}{\epsilon} \left(\frac{\sinh \kappa a}{\kappa a}\right)^2 \frac{e^{-\kappa R_{mn}}}{R_{mn}} \qquad R_{mn}\geq 2a \quad , \qquad (2.5)$$

where κ is the inverse screening length based on the average concentration of small ions (n_{io}) with charge number Z_i, that compensate the charges on the macroions:

$$\kappa^2 = \frac{4\pi e^2}{\epsilon k_B T} \sum_i n_{io} z_i^2 \qquad \text{and} \qquad \sum_i n_{io} z_i^2 + \frac{1}{V}\sum Z=0 \quad , \qquad (2.6a,b)$$

V being the volume of solution. It is clear that the E_{self} and V_n^F are independent on the positions of the particles, whereas U_{mn}^F contains the relative positions of particles explicitly ($R_{mn}=|R_m-R_n|$). It is

interpreted as an effective macroion-macroion potential.

Sogami calculated next the *Gibbs* free energy G from the relation

$$G = [\sum_i n_{io}(\frac{\partial F}{\partial n_{io}})_{V,T}]_{V=V(T,P)} \quad , \qquad (2.7)$$

including a contribution from macroions on account of the charge neutrality condition (eq.2.6b). Then for N identical macroions, eaqch with charge Z, G is written as

$$G = [\sum_i n_{io}(\frac{\partial F}{\partial n_{io}})_{V,T,Z} + N\ Z\ (\frac{\partial F}{\partial Z})_{V,T,N}] \quad , \qquad (2.8)$$

which leads to

$$G = G' + 2E_{self} + \sum_n V_n^G + 1/2 \sum_{m \neq n} U_{mn}^G \quad , \qquad (2.9)$$

where

$$V_n^G = \frac{(Ze)^2}{4\epsilon\kappa a^2}\ (3/2(1-e^{-2\kappa a}) + \kappa a e^{-2\kappa a} - 4\kappa a) \quad , \qquad (2.10)$$

and

$$U_{mn}^G = U_{mn}^F (1 + \kappa a \coth \kappa a - \frac{1}{2}\ \kappa R_{mn}) \quad , \qquad (2.11)$$

This is negative above certain value of R_{mn}, implying attraction between particles, and has a minimum at

$$R_{mn} = \{\kappa a \coth \kappa a + 1 + [(\kappa a \coth \kappa a + 1)(\kappa a \coth \kappa a + 3)]^{1/2}\}/\kappa$$

which moves depending on κ and a.

3. Linear response and effective potential from Helmholtz free energy:

In this section we will show how the definition of the effective interactions between polyions can be given within a general framework of linear response theory, allowing for polyion-counterion interactions which are not merely electrostatic in nature at short distance (through *Fourier*-trasformable) and without necessarily involving the *Poisson-Boltzmann* equation. The relevant information needed for this work is the structure of the counterion fluid, as summarized in its partial liquid structure factors.

We consider for simplicity a macroion-counterion interaction which is given by

$$V_{ext}(r) = \frac{zZe^2}{\epsilon}\left(\sum_l \frac{1}{|r-R_l|}\, \theta(|r-R_l|-a)+C\theta(a-|r-R_l|)\right) \quad , \qquad (2.12)$$

where Z(z) are the valency of the macroion (counterion) respectively, and R_l is the position of the Lth macroion. The above potential represents *Coulomb* interactions outside the macroion core and a constant interaction (denoted by C) inside the core. The *Fourier* transform of $V_{ext}(r)$:

$$V_{ext}(k) = \int e^{-ik.r} V_{ext}(r)\, dr$$

$$V_{ext}(k) = \frac{4\pi zZe^2}{\epsilon k^2}\{(1-aC)\cos ka + \frac{C}{k}\sin ka\}\sum_l e^{-ik.R_l} \quad ,(2.13)$$

If $V_{ext}(r)$ is weak enough that we can work within linear response theory, then the change of the counterion charge density $\delta q(k)$[60] is

$$\delta q(k) = Ze\chi(k)V_{ext}(k) \quad , \qquad (2.14)$$

Here, $\chi(k)$ is the density-density response function, which is directly related to the structure factore $S(k)$. The relation between $S(k)$ (a direct measure of the density fluctuations in the system) and the static response function $\chi(k)$ follows for a classical system from the fluctuation-dissipation theorem, and reads

$$\frac{1}{\epsilon(k)} = 1+\frac{4\pi Z^2 e^2}{k^2}\chi(k)$$

$$= 1-\frac{4\pi Z^2 e^2 \bar{n}}{k^2 k_B T} S(k) \qquad , \qquad (2.15)$$

where $\bar{n}$ is the average density of the counterions. Thus, knowing $S(k)$ one can calculate the induced charge density $\delta q(k)$ and hence the electrostatic energy of the solution as a function of the configuration of the macroions.

In the *Debye-Hückel* limit one has

$$S(k) \longrightarrow S_{DH}(k) = \frac{k^2}{k^2+\kappa^2} \qquad , \qquad (2.16)$$

with the *Debye* screening length κ^2. Hence, from the *Poisson* equation

$$\epsilon k^2 \phi(k) = 4\pi Ze\sum_l \rho_l(k) + 4\pi ze\chi_{DH}(k)V_{ext}(k) \qquad , \qquad (2.17)$$

one finds

$$\phi(k) = \frac{4\pi Ze}{\epsilon k^2}\left[\frac{\sin ka}{ka} - \frac{\kappa^2}{k^2+\kappa^2}\left\{(1-aC)\cos ka+\frac{C}{k}\sin ka\right\}\sum_l e^{-ik.R_l}\right. \qquad (2.18)$$

where C has the dimension of length, and it will be considered as three different values (1/a;0;-1/a), where in the case with C=1/a we will recover *Sogami's* work with a negative constant effective interaction ($\beta v_{12}(r)$) inside the macroion "core".

From equation (2.17), this is clearly the sum of a term $\phi^1(k)$ due to the macroions and a term $\phi^2(k)$ due to the screening ions. Hence, the electrostatic energy E_c of the system as a function of particle coordinates R_l is given by

$$E_c = \frac{1}{2}\int dr\ \delta q(r)\phi^2(r) + \frac{1}{2}\int dr\ \rho_l(r)\phi^1(r) + \int dr\ \delta q(r)V_{ext}(r)/ez \tag{2.19}$$

Explicit evaluating yields

$$E_c = \frac{1}{2}\sum_{ll'} U_c(R_{ll'}) + \sum_l V_c \quad , \tag{2.20}$$

where

$$V_c = \frac{Z^2e^2}{4\epsilon}\ [(1-aC)\{a\kappa^2 e^{-2\kappa a} - 3\kappa(1+\frac{1}{2}\ e^{-2\kappa a})\}$$

$$= +C^2\{ae^{-2\kappa a} + \frac{1}{2\kappa}\ (1-e^{-2\kappa a})\} + C(1-aC)\{\kappa a e^{-2\kappa a} - e^{-2\kappa a}\}]\ , \tag{2.21}$$

and

$$U_c(R) = \frac{Z^2e^2}{\epsilon R}\ e^{-\kappa R}[(1-aC)^2 ch^2\kappa a(1-\frac{1}{2}\ \kappa R + \kappa a\ tgh\kappa a)$$

$$= +2C^2\frac{\sinh^2\kappa a}{\kappa^2}\ (-\frac{1}{4}\ \kappa R + \frac{1}{2}\ \kappa a\ \coth\kappa a)$$

$$= +\frac{2C(1-aC)}{\kappa}\ ch\kappa a\ \sinh\kappa a(1 - \kappa R + \kappa a\ \coth\kappa a + \kappa a\ tgh\kappa a)] \tag{2.22}$$

The *Helmholtz* free energy follows by integrating $E_c = e^2(\partial F/\partial e^2)_{V,T}$ with respect to e^2 from 0 to e^2

$$F = F^o + \frac{1}{2}\sum_{ll'} U_F(R_{ll'}) + \sum_l V_F \quad , \tag{2.23}$$

where

$$U_F(R) = \frac{Z^2e^2}{\epsilon R} e^{-\kappa R} [(1-aC)^2 ch^2\kappa a + 2C^2 \frac{\sinh^2\kappa a}{\kappa^2}$$

$$+ \frac{2C(1-aC)}{\kappa} \sinh \kappa a \text{ ch } \kappa a] \quad , \qquad (2.24)$$

and

$$V_F = \frac{Z^2e^2}{\epsilon} [2(1-aC)\kappa(-1- \frac{1}{2} e^{-2\kappa a}) + \frac{C^2}{\kappa} (1-e^{-2\kappa a}) - C(1-aC)e^{-2\kappa a}] \qquad (2.25)$$

At this point we would like to illustrate the effect of the "amplitude factor" in the *Yukawa* potential for different values of the constant C, comparing with the value adopted in the work of *Shih et al.* discussed in section 5.2 of chapter 1. Figure 2.1 represents various results for the amplitude factor f as a function of κa, in the following cases:

(1) $f = ch^2\kappa a$ for C=0

(2) $f = \frac{\sinh^2\kappa a}{(\kappa a)^2}$ for $C = \frac{1}{a}$ (recovering *Sogami's* work)

(3) $f = 4ch^2\kappa a + \frac{\sinh^2\kappa a}{(\kappa a)^2} - \frac{4}{\kappa a} ch\kappa a \sinh\kappa a$ for $C = -\frac{1}{a}$

(4) $f = \left(\frac{e^{\kappa a}}{1 + \kappa a}\right)$ for *Shih et al.* work

It is clear from the figure that there is great uncertainity in the strength of the effective repulsion (i.e. the effective charge) between macroions.

In spite of the sensitivity of the "amplitude factor" to the detailed assumption on the short-range interaction between macroions and counterions, we note that, if we follow *Sogami's* procedure to

evaluate the *Gibbs* free energy and hence the effective potential between macroions, the position of the minimum in its attractive well is essentially insensitive. This is shown in table (2.1).

4. From Helmholtz free energy to Gibbs free energy:

In order to calculate the *Gibbs* free energy G, one need to know the chemical potential μ_j given by

$$\mu_j = \left(\frac{\partial F}{\partial N_j}\right)_{V,T,N_{i\neq j}} \quad , \qquad (2.26)$$

where F is the *Helmholtz* free energy and N_j is the number of molecules (or ion) of component j. Then G is given by

$$G = \sum_j N_j \mu_j \quad , \qquad (2.27)$$

the sum being over all components of the system.

In section 2 we have seen that *Sogami's* calculation for the *Gibbs* free energy, the chemical potential of the solvent is ignored, results in an attractive potential between macroions in their $U^G_{mn}(R)$ (eq.2.10). Recently it was claimed by *Overbeek*[57] that one should include the role of the solvent in the *Gibbs* free energy and on doing so the attractive part in $U^G_{mn}(R)$ will disappear. He writes

$$G = N_{solv}\mu_{solv} + \sum_i N_i \mu_i + G_{part} = F + PV \quad , \qquad (2.28)$$

where G_{part} is the contribution of macroions. Using

$$\mu_j = \left(\frac{\partial F}{\partial N_j}\right)_{P,T} + P\left(\frac{\partial V}{\partial N_j}\right)_{P,T} \quad , \qquad (2.29)$$

and dealing first with the contribution of the solvent and the counterion, he writes

$$N_{solv}\mu_{solv} + \sum_i N_i\mu_i = N_{solv}\left(\frac{\partial F'}{\partial N_{solv}}\right)_{P,T} + \sum_i N_i\left(\frac{\partial F'}{\partial N_i}\right)_{P,T}$$

$$+ PN_{solv}V_{solv} + P\sum_i N_i V_i + N_{solv}\left(\frac{\partial F^{el}}{\partial N_{solv}}\right)_{P,T} + \sum_i N_i\left(\frac{\partial F^{el}}{\partial N_i}\right)_{P,T}$$

$$= F'_{solut} + PV_{solut} + \frac{\partial F^{el}}{\partial(\kappa^2)}\{N_{solv}V_{solv}\frac{\partial(\kappa^2)}{\partial V_{solut}}$$

$$+ \sum_i N_i(V_i\frac{\partial(\kappa^2)}{\partial V_{solut}} + \frac{\partial(\kappa^2)}{\partial N_i})\}$$

$$= G'_{solut} + \frac{\partial F^{el}}{\partial(\kappa^2)}\{-V_{solut}\frac{\kappa^2}{V_{solut}} + \kappa^2\} = G'_{solut} \quad .(2.30)$$

Here, the *Helmholtz* free energy has been writen as

$$F = F' + F^{el}$$

F' being the free enrgy of the discharged system and F^{el} being due to charging process. The subscript (solut) includes the solvent and the counterions, but not the macroions. V_j represents the molecular volume of j. Note that $F^{el} \neq 0$, but $V^{el} = 0$, since V^{el} means the change in volume during the charging process conducted at constant numbers of ions and solvent molecules, with all macroions at fixed positions, R_n.

This result shows that the solvent and the small ions together give a zero contribution to G^{el}. The same result can be obtained from *Gibbs-Duhem* relation in the solution which states that

$$N_{solv}\mu^{el}_{solv}+\sum_i N_i\mu^{el}_i = \int_{e=0}^{e=e} (N_{solv}d\mu^{el}_{solv}+\sum_i N_i\mu^{el}_i)_{P,T} = 0 \quad . \quad (2.31)$$

The term $-\kappa R$ in eq.(2.11), which resulted in the attraction between the particles has its origin in the term $\kappa^2(\partial F^{el}/\partial(\kappa^2))$, derived from $\sum_i N_i\mu_i$ in eq.(2.28). Now this term is exactly canceled by the corresponding term derived from the contribution of the solvent as shown in eq.(2.30) and (2.31) and thus the attraction in G disappears.

Adding the contribution of the macroion to G, one has

$$G_{total} = G'_{solut}+G'_{part}+G^{el}_{part}$$

$$=F'+PV_{solut}+PV_{part}+F^{el}= G'_{total}+F^{el} \quad , \quad (2.32)$$

and thus

$$G^{el}_{part}(=G^{el}_{total}) = F^{el} \quad , \quad (2.33)$$

and in particular

$$U^G_{mn} = U^F_{mn} \quad . \quad (2.34)$$

Thus the interaction between the macroions is the same at constant T and P as it is at constant T and V and thus the interaction is a pure repulsive (within the *Debye-Hückel* theory, ofcourse).

In conclusion, it appears that, as long as one is relying on the *Debye-Huckel* approximation and linear response theory, the condensation phenomena do not have a simple explanation. A possible line of further study is to see whether an effective attraction between macroions may arise from the *Helmholtz* free energy alone once the character of the

screening becomes oscillatory. This question could be examined within linear response theory, but clearly transcending the *Debye-Hückel* theory. A more appealing approach of immediate interest involves treating the macroions and microions on equal footing, returning to the hard core potential and treating the solvent as a uniform dielectric medium. Such a study of condensation (gas-liquid) coexistence will be the main subject of chapter 3.

	U_G(Rmin) eV			Rmin $\times 10^3 A^\circ$			$R_{exp} \times 10^3 A^\circ$
κa	C=1/a	C=0	C=-1/a	C=1/a	C=0	C=-1/a	
0.48	-0.5	-0.42	-0.36	17.7	18.7	19.5	18
0.58	-0.56	-0.44	-0.37	15.3	16.5	17.4	15
0.92	-0.74	-0.46	-0.37	10.0	11.5	12.5	10
1.50	-0.74	-0.41	-0.40	7.0	8.6	9.3	8

Table 2.1: Comparison of the calculated distance Rmin and the observed interparticle distance R_{exp} [62] in dilute collidal suspension of charged (charge number $Z=4\times10^3$) and spherical (redius a=1705 A°) polymer particles for different particle concentration and different values of the constant C.

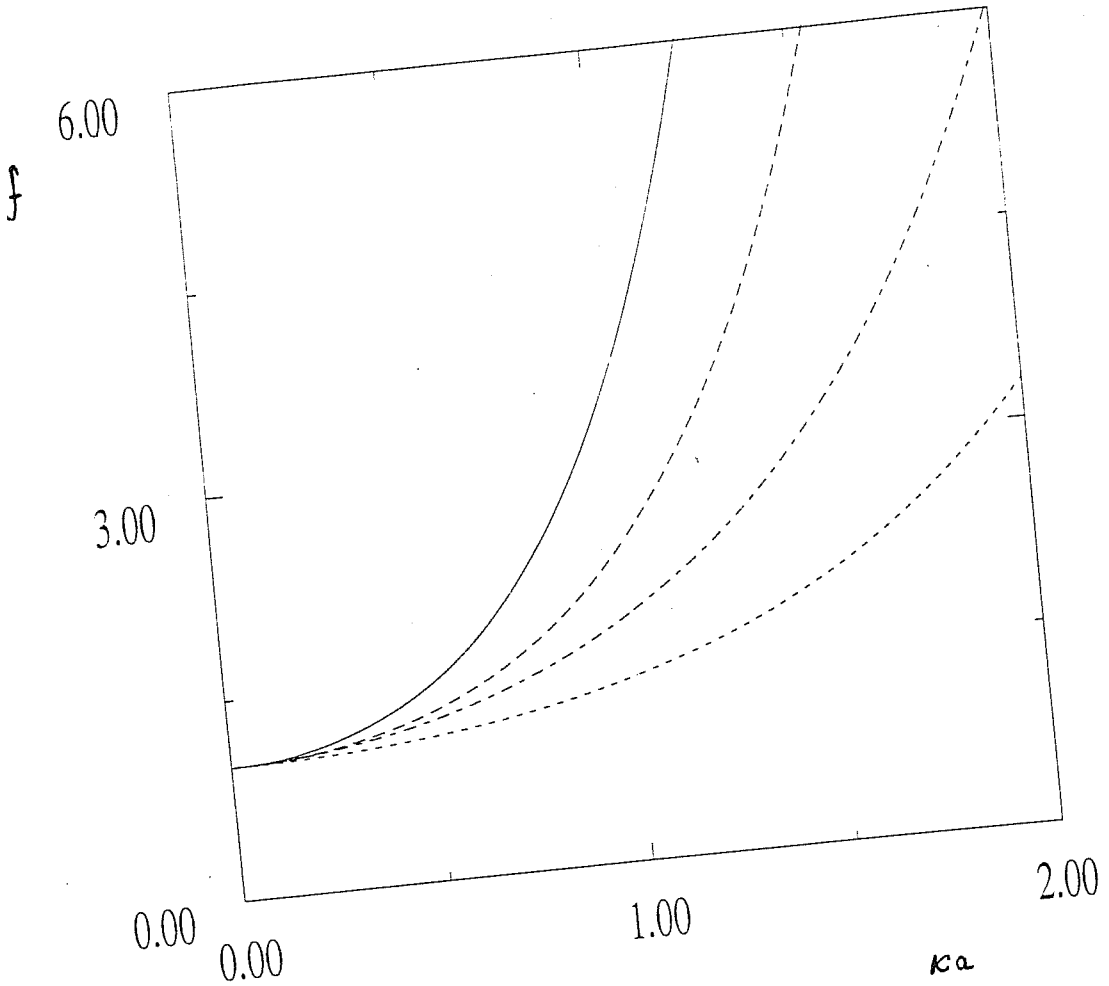

Fig.2.1.: The amplitude form factor as a function of κa.(——) for C = -1/a; (---) for C = 0; (-.-.-.) for *Shih et al.* work; and [illegible] Sogami's work).

CHAPTER III

GAS-LIQUID TRANSITION IN HIGHLY ASYMMETRIC POLYELECTROLYTES

1. Introduction:

The aim of this chapter is to construct gas-liquid coexistence curves for a two-component liquid of charged hard spheres with very different charges and sizes. We use the mean spherical approximation (MSA), which has the advantage of providing analytical expresions for the thermodynamic quantities. Recalling the discussion of the existence of two phases in section (5.4) of chapter 1, *Belloni*[54] had studied highly asymetric polyelectrolytes using the hypernetted chain approximation (HNC), by which he was able to construct a spinodal line between two phases, interpreted as a plasma-like phase (at low density) and a liquid-like phase (at high density). In this chapter we will compare the results of *Belloni* with our predicted values for the critical temperature and the spinodal line. In addition, however, we shall give the liquid-gas coexistence curve. We shall be using the same values for charges and diameter in the charged fluid as *Belloni* did.

Fluid systems of charged hard spheres have been intensively studied in the past for their intrinsic statistical-mechanical interest and for their ability to represent physical systems. Fluids of charged hard spheres in a neutralizing background have been studied and the solution of the mean spherical approximation is known[62], first of

all, for the case of a one-component system. The extension of the model to mixtures of charged hard spheres in a uniform background has been concidered by *Bhuiyan* and *March*[63] in a limiting case. The general solution of the MSA for an arbitrary multi-component fluid of charged hard spheres in a uniform neutralizing background was obtained by *Parrinello* and *Tosi*[64], by a method which relies on the factorization scheme of *Baxter*[65] as extended to charged fluid by *Blum*[66].

In section 2 we will use the general solution of the MSA[64] for a two-component system, by which we shall construct the liquid-gas coexistence curve for the system of present interest. In section 3 we shall discuss the effect of the size ratio between macroions and counterions on the critical temperature and the critical volume fraction, and how the MSA fares in its predictions relative to *Belloni's* HNC work. Finally in section 4 we shall discuss the problem of coexistence between the two phases of the system.

2. Thermodynamic properties in the mean spherical approximation:

The model system that we consider is a two-component system of charged hard spheres (macroions) and point-like or almost point-like charges (counterions), both embedded in a dielectric medium which is taken into account by a dielectric constant ϵ which reduces the bare *Coulombic* interaction between particles and counterions. The macroions have a diameter σ_1, charge z_1, and number density ρ_1, whereas the counterions have diameter σ_2, charge z_2 and number density ρ_2. The

constraint imposed by the overall electroneutrality is $\rho_1 z_1 + \rho_2 z_2 = 0$. The MSA imposes the following conditions on the total correlation function $h_{ij}(r)$:

$$h_{ij}(r) = -1 \qquad (r<\sigma_{ij}) \quad , \qquad (3.1)$$

and the direct correlation functions $c_{ij}(r)$

$$c_{ij}(r) = -z_i z_j \beta e^2/\epsilon r \qquad (r>\sigma_{ij}) \quad , \qquad (3.2)$$

where $\sigma_{ij}=1/2(\sigma_i+\sigma_j)$ and $\beta=1/k_B T$. Condition (3.1) is exact for hard spheres. A quantity of direct physical measuring in the MSA is the parameter Γ, which has the dimension of an inverse length and 2Γ approaches the *Debye* inverse length κ_o from below for infinite dilution.

The parameter Γ is to be determined by solving the equation

$$2\Gamma = \alpha \left(\sum_i \rho_i \left[\frac{z_i - (\pi/2\Delta)\sigma_i^2 P_n^2}{1 + \Gamma\sigma_i} \right]^2 \right)^{1/2} \quad , \qquad (3.3)$$

selfconsistently, where

$$\Delta = 1 - \frac{\pi}{6} \zeta_3 \qquad (3.4)$$

$$\zeta_m = \sum_{i=1}^{2} \rho_i \sigma_i^m \qquad (3.5)$$

$$\alpha^2 = 4\pi\beta e^2/\epsilon_o \quad , \qquad (3.6)$$

and

$$P_n = \Omega^{-1} \sum_{i=1}^{2} [\rho_i z_i \sigma_i/(1 + \Gamma\sigma_i)] \qquad (3.7)$$

with

$$\Omega^{-1} = 1 + (\pi/2\Delta) \sum_{i=1}^{2} [\rho_i \sigma_i^3/(1 + \Gamma\sigma_i)] \qquad (3.8)$$

The numerical solution of equation (3.3) can be obtained from either the *Newton-Raphson* formula or by simple iteration starting from some guessed initial value of Γ.

The MSA provides an analytic expression for the excess internal energy ΔE, which is given by

$$\frac{\epsilon\ \Delta E}{e^2} = -\left[\Gamma \sum_{i=1}^{2} [\rho_i \sigma_i^2/(1 + \Gamma\sigma_i)] + \frac{\pi}{2\Delta}\ \Omega\ P_n^2 \right] \quad , \qquad (3.9)$$

as well as for the excess free energy,

$$\beta\Delta A = \beta\Delta E + \Gamma^3/3\pi \quad . \qquad (3.10)$$

Finally, the excess pressure can be obtained from the following relation

$$\beta\Delta P = \zeta_o^2 \left[\frac{\partial(\beta\Delta A/\zeta_o)}{\partial\zeta_o} \right]_T \quad , \qquad (3.11)$$

and the results reads

$$\beta\Delta P = -\Gamma^3/3\pi - (\alpha^2/8\Delta^2)P_n^2 \quad . \qquad (3.12)$$

In order to calculate the equation of state one needs to add the hard sphere contribution, P_o, calculated from the PY compressibility of the hard-sphere fluid;

$$\beta P_o = \frac{6}{\pi} \left[\frac{\zeta_o}{1 - \zeta_3} + \frac{3\ \zeta_1\zeta_2}{(1 - \zeta_3)^2} + \frac{3\ \zeta_2^3}{(1 - \zeta_3)^3} \right] \quad , \qquad (3.13)$$

then the equation of state is

$$\beta P = \Omega_o - \Gamma^3/3\pi - (\alpha^2/8\Delta^2)P_n^2 \quad , \quad (3.14)$$

using this equation of state we can now obtain the isotherms of the sustem for different temperatures.

3. Numerical results for isotherms and liquid vapour critical points:

We consider first the case in which the macroions have diameter σ_1=60°A and valency z_1=20, whereas the counterions have valency z_2=-1 and diameter σ_2=0 (micelle≡system 1). The equation of state (eq.3.14) is plotted for different values of temperature (using reduced pressure $P^*=\epsilon P\sigma_1^4/e^2$ and reduced temperature $T^*=2\pi\sigma_1/\alpha^2$) as a function of the volume fraction occupied by the macroions which is $\Phi=\frac{\pi}{6}\rho_1\sigma_1^3$.

The isotherms of the model have the classical *van der Waals* shape with a liquid-gas critical point (fig. 3.1). We can see that the predicted critical temperature is lower than the one predicted using the HNC by *Belloni*; whereas the critical volume fraction in our calculation is higher (table 3.1). Also in figure (3.1) we have plotted the spinodal line. From the charged hard sphere fluid studies[52] using the MSA it was concluded that the MSA yields good values of the critical temperature and density, and yields instead a value of the critical pressure that is too low when compared with best available estimates[51].

In figure (3.2) we illustrate how the shape of the isotherms is modified on varying the ratio σ_1/σ_2. It is clear that the critical

temperature increases as the ratio σ_1/σ_2 increases for the same valency ratio $|z_1/z_2|=20$.

Belloni[67] has considered another valency ratio for different diameter ratio ($\sigma_{1,2}$=50,5; $z_{1,2}$= -40,1), using the mixed integral equation proposed by *Zerah* and *Hansen*[68] to highly asymmetrical polyelectrolytes within the primitive model. This approximate theory interpolates continuously between the *Percus-Yevick* and the Hypernetted chain theories for charges of the same sign and between HNC and MSA for charges of opposite sign. In his results the two-phase region in the phase diagram was shifted towards lower temperatures.

Considering now the same valency ratio and diameters ratio as in ref.(67) (≡system 2), we show the isotherms given by the MSA in figure (3.3). Hence with point-like (almost point-like) counterions, with different valency ratio (system 1 and system 2) the critical temperature is increased, while the gas phase lies in a narrower region.

In the following section we will discuss the way that we used to locate the coexisting curve for the different cases.

4. Coexistence curve:

The coexistence curve can next be determined by imposing the equality of the chemical potential μ in both phases. Knowing the excess free energy per unit volume from equation (3.10), and the excess free energy of neutral hard spheres obtained by integrating equation (3.13)

with respect to the volume (at constant temperature), i.e.

$$\frac{\beta A^{ex}}{N_1} = \int \left(\frac{\beta P_o}{\rho_1} - 1\right) \frac{d\rho_1}{\rho_1}$$

$$= -(1-z_1)\ln|1-\zeta_3| + \frac{3S_1S_2}{S_3}\left(\frac{\zeta_3}{1-\zeta_3}\right) - \frac{S_2^3}{S_3^2}\left(\frac{3\zeta_3^2}{2(1-\zeta_3)^2}\right) , \quad (3.15)$$

where

$$S_1 = \sigma_1 - z_1\sigma_2 \quad ; \quad S_2 = \sigma_1^2 - z_1\sigma_2^2 \quad ; \quad S_3 = \sigma_1^3 - z_1\sigma_2^3 \quad ,$$

then the *Helmholtz* free energy per unit formula is given by

$$\beta F = \beta F_{ideal} + \frac{\beta\Delta A}{\rho_1} + \frac{\beta A^{ex}}{N_1} \quad (3.16)$$

where βF_{ideal} is the *Helmholtz* free energy per unit formula for the ideal system given by[59]

$$\beta F_{ideal} = \ln\rho_1 + z_1\ln\rho_2 + f(T) \quad . \quad (3.17)$$

The function f(T) is only a function of temperature and will cancel out when equilibium between two phases at the same temperature is imposed. Finally, μ=G/N where the *Gibbs* free energy is obtained as

$$G = F + PV \quad , \quad (3.18)$$

using equations (3.17,16,15,10,9 and 3.14).

With the aid of equation (3.18), we were able to impose the equality of the chemical potentials of the two phases analytically, and hence to plot the coexistence curve (fig. 3.1 and 3.3).

In summary, using the MSA we have studied the condensation of a highly asymmetric polyelectrolyte in the transition from a plasma-like phase to a condensed liquid-like phase. We have explicitly demonstrated

that there exists a coexistence curve governing the thermodynamic equilibrium between the two phases. The predicted critical temperature and volume fraction depend very much on the approximate fluid-state theory being used for a given model system.

We replot our results for the coexistence and spinodal curves of system 1 in figure (3.4) on a plot where the variables $1-T^*/T_c^*$ and Φ/Φ_c are used. This type of plot very sensitively displays the behaviour of the curves near the citical point. Clearly, we shall have to refine our numerical procedures in this region ($T^*/T_c^* \longrightarrow 1$) and to extend the calculations closer to the critical point. The aim will be to evaluate the critical exponent β in the asymptotic relation;

$$\frac{\Phi_l - \Phi_g}{\Phi_c} = \text{constant.}\left[1 - T^*/T_c^* \right]^{\beta} \qquad (3.19)$$

which is valid close to the critical point. We expect that the MSA theory, being a mean field theory which does not take proper account of critical fluctuations, will yield $\beta=1/2$.

	MSA		HNC	
	T_c^*	Φ_c	T_c^*	Φ_c
$z_1=20$; $z_2=-1$				
$\sigma_1=60^\circ A$; $\sigma_2=0^\circ A$	1.056	0.03	4.25	0.006
$z_1=-40$; $z_2=1$				
$\sigma_1=50^\circ A$; $\sigma_2=5^\circ A$	1.818	0.0008	——	——

Table 3.1.: Predicted reduced temperature and volume fraction compared with the HNC values[57].

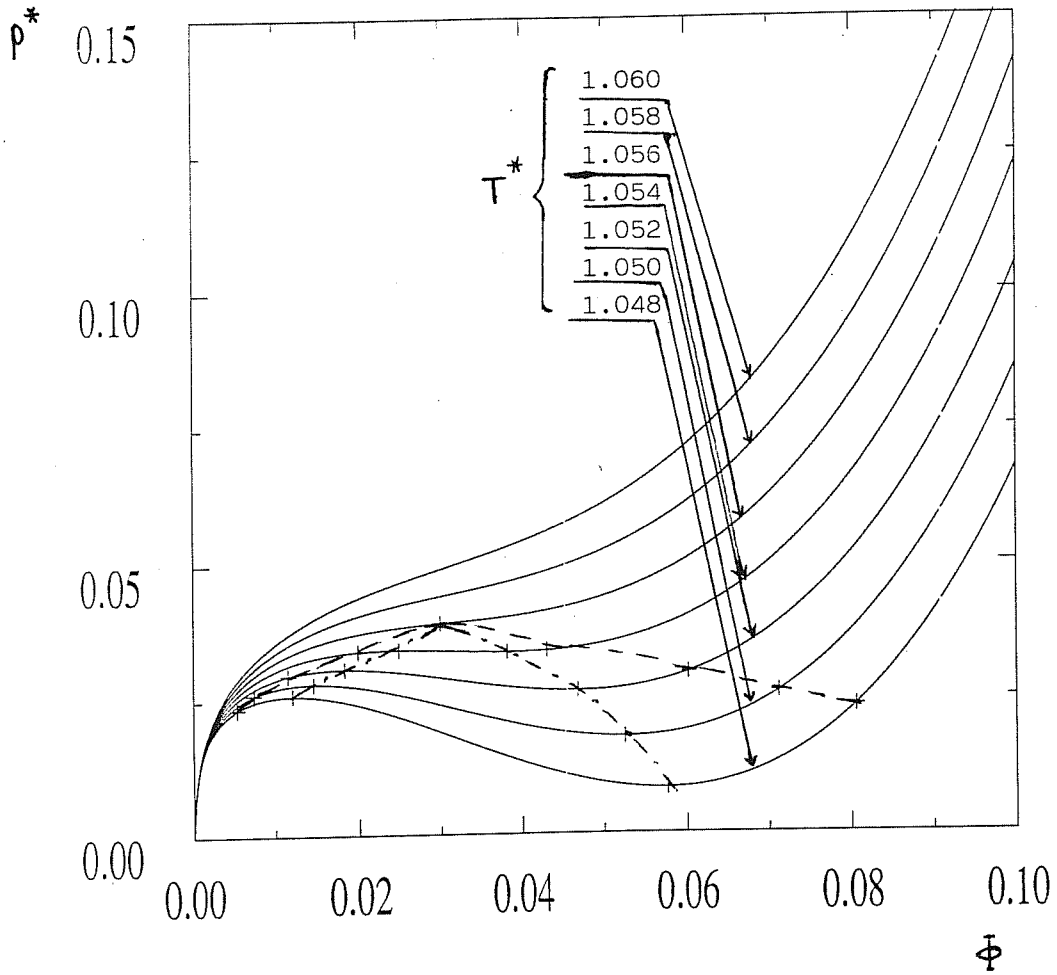

Fig. 3.1.: Isotherms (full curve) for different reduced temperature, as labelled. For the ratio $\sigma_1/\sigma_2=\infty$ (system 1) and $|z_1/z_2|=20$. (----) the coexistence curve; and (-.-.-.) the spinodal line.

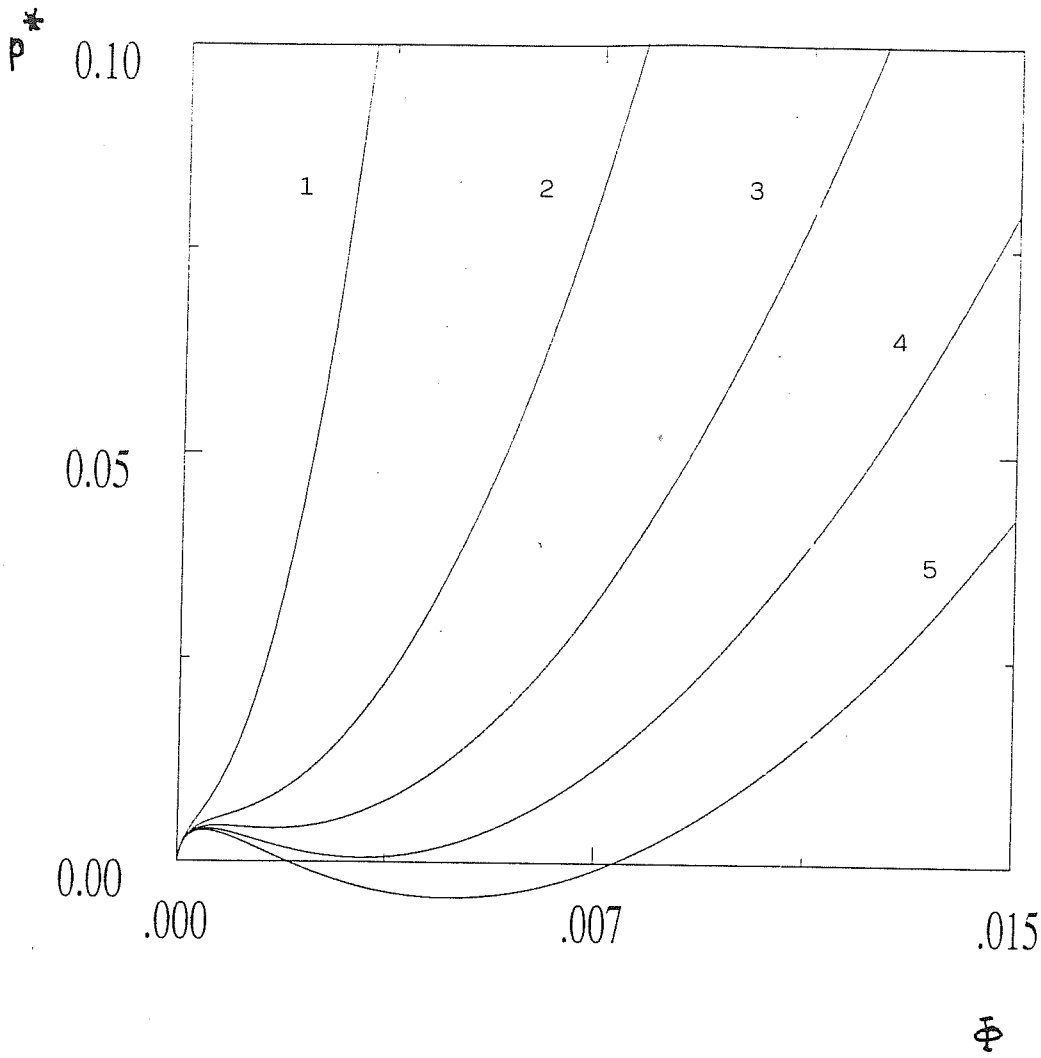

Fig. 3.2.:Isotherms (full curve) of the model for the ratio $|z_1/z_2|=20$; with different size ratio σ_1/σ_2 as labelled and reduced temperature $T^*=0.895$.

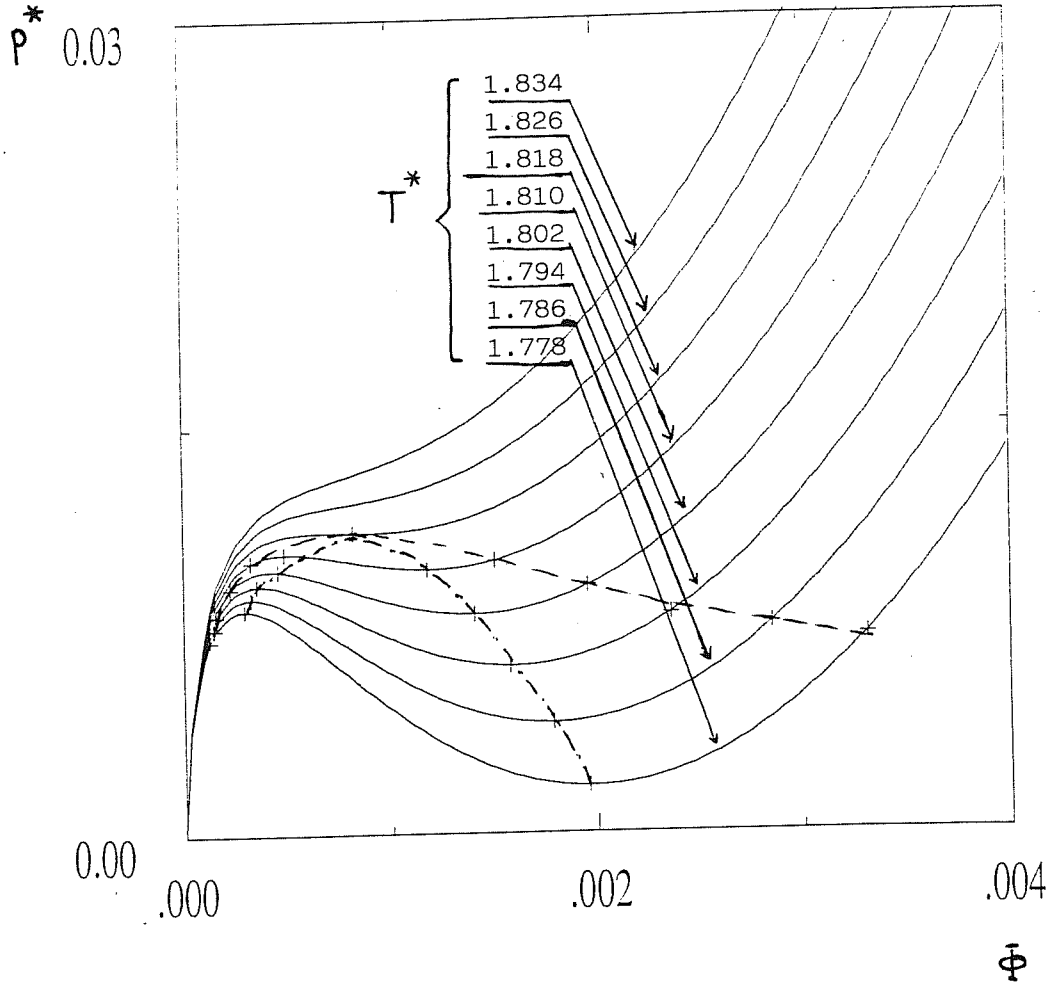

Fig. 3.3.: Isotherms (full curve) for different reduced temperature, as labelled. For the ratio σ_1/σ_2=10 (system 2) and $|z_1/z_2|$=40. (----) the coexistence curve; and (-.-.-.) the spinodal line.

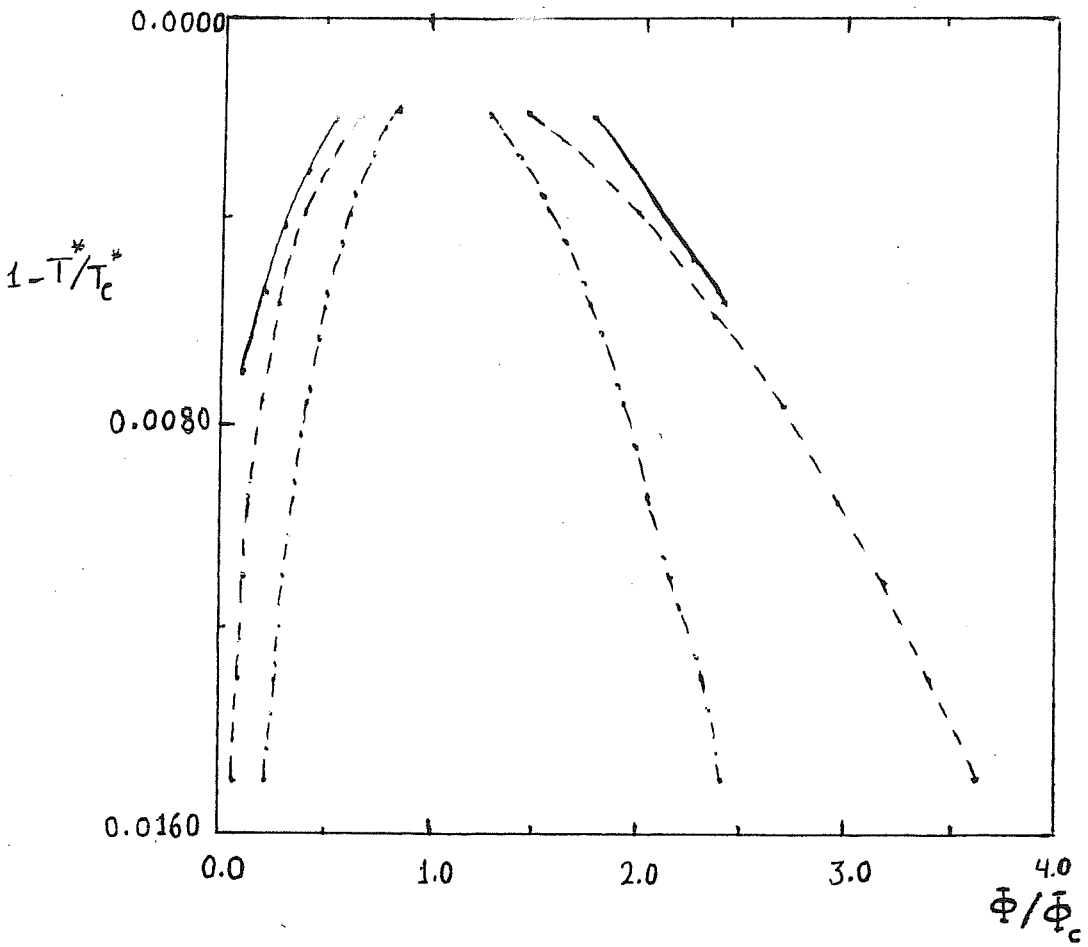

Fig. 3.4.: Liquid-gas coexistence curve (----). Spinodal line (-.-.-.) compared with the spinodal line of *Belloni*[54] (———).

REFERENCES:

1. F.Selmi, Nuovi Ann. Science Nature di Bologna (2), 4, 146(1845); 8, 404(1847); Ann. di Majocchi, 15, 88,235(1844); 24, 225(1846).

2. M.Faraday, Phil. Trans. Royal Soc., 147, 145(1857).

3. Th.Graham, Phil. Trans. Royal Soc., 151, 183(1861).

4. P.Pieranski, Contemp. Phys., 24, 1(1983).

5. J.Th.G.Overbeek "Colloidal Dispersions" ed.;J.W.Goodwin, The Royal Society of Chemistry, Burlington House, London W1VOBN, 1981.

6. J.Perrin, "Le Atomes" 9 me mille, Libr. ed.; F.Alcan, Paris, 1920.

7. A.A.Caljé, W.G.M.Agterof and A.Vrij, in "Micellization, solubilization and Microemulsions" ed.; K.L.Mittal, Plenum Press, N.Y. 1977, vol 2 P.799.

8. M.Von Smoluchowski, Physik Z., 17, 557(1916); Z. Physik. Chem., 92, 129((1917).

9. B.V.Deryagin and V.M.Müler, Dokel. Akad. Nauk. S.S.S.R. (Engl. Transl.), 176, 738(1967).

10. L.A.Spielman, J. Colloid Interface Sci, 33, 562(1970).

11. E.P.Honig, G.J.Robersen and P.H.Wiersema, J. Colloid Interface Sci, 36, 97(1971).

12. J.M.Deutch and B.U.Felderhof, J. Chem. Phys., 59, 1669(1973).

13. J.W.Th.Lichtenbelt, H.J.M.C.Ras, and P.H.Wiersema, J. Colloid Interfaces Sci., 46, 522(1974); J.W.Th.Lichtenbelt, C.Pathmamanoharan, and P.H.Wiersema, 49, 281(1974).

14. S.Hachisu, Y.Kobayashi and A.Kose, J.Colloid Interface Sci., 42, 342(1973).

15. J.G.Kirkwood, J.Chem. Phys., **7**, 919(1939); B.J.Alder and F.E.Wainright, Phys. Rev., **127**, 359(1962).

16. R.C.Williams and K.Smith, Nature, **4551**, (1957) London 1.

17. P.J.Darragh, A.J.Gaskin and T.V.Sanders, Scient. Am., **234**, 84(1976).

18. W.Ströber, A.Fink and E.Bohn, J. Colloid Interface Sci., **26**, 62(1968).

19. D.J.Shaw, "Introduction to Colloid and Surface chemistry" 2nd ed.: Butterworths London-Boston 1980.

20. P.N.Pusey, "Colloidal Dispersion" ed.:J.W.Goodwin, The Royal Society of Chemistry Burlington House. London W1VOBN 1981.

21. N.Ise and T.Okubo, Acc. Chem. Res., **13**, 303(1980).

22. R.Williams and R.S.Crandall, Phys. Lett. **A 48**, 225(1974).

23. N.Ise, T.Okubo, S.Kunugi, H.Matsuoka, K.Yamamoto and Y.Ishii, J.Chem. Phys., **81**, 3294(1984).

24. T.Yoshiyama and I.Sogami, Phys. Rev. Lett., **53**, 2153(1984).

25. D.J.W.Aastuen, N.A.Clark and L.K.Cotter, Phys. Rev. Lett., **57**, 1733(1986).

26. Chuan-Fu Wu and Sow-Hsin Chen, J. Chem. Phys., **87**, 6199(1987).

27. R.H.Ottewill, "Colloid Dispersion" ed.: J.W.Goodwin, The Royal Society of Chemistry, Burlinton House, London W1VOBN 1981.

28. E.J.W.Verwey and J.Th.G.Overbeek, "Theory of the Stability of Lyophobic Collids" Elsevier, Amsterdam 1948.

29. F.London, Zeit. Phys., **63**, 245(1930).

30. D.Tabor, "Colloidal Dispersion" ed.: J.W.Goodwin, The Royal Society of Chemistry, Burlington House, London W1VOBN 1981.

31.W.G.Hoover and M.Ross, Contemp. Phys., **12**, 339(1971).

32. W.G.Hoover and F.H.Ree, J. Chem. Phys., **47**, 4873(1967).

33. K.Takano and S.Hachisu, J. Chem. Phys., **67**, 2604(1977).

34. J.Alder, W.G.Hoover and D.A.Young, J. Chem. Phys., **49**, 3688(1968).

35. W.G.Hoover, S.G.Gray and K.W.Johnson, J. Chem. Phys., **55**, 1128(1971).

36. H.Riess, S.W.Mayer and J.L.Katz, J. Chem. Phys., **35**, 820(1961); N.H.March and M.P.Tosi, Phys. Chem. Liquids, **10**, 185(1980).

37. K.Fuch, Proc. Roual Soc., **A 151**, 585(1935).

38. N.H.March and M.P.Tosi, "Coulombic Liquids" Acadamic Press, London, N.Y. 1984.

39. J.G.Kirkwood and E.Monroe, J. Chem. Phys., **8**, 845(1940).

40. T.V.Ramakrishnan and M.Yussof, Phys. Rev., **B 19**, 2775(1979).

41. A.D.J.Haymet and D.W.Oxtoby, J. Chem. Phys., **74**, 2559(1981).

42. M.Rovere and M.P.Tosi, J. Phys. C, (1985).

43. Wei-Heng Shih and D.Stroud, J. Chem. Phys., **79**, 6254(1983).

44. Wan Y.Shih, IIhan A. Aksay and R.Kikuchi, J. Chem. Phys., **86**, 5127(1987).

45. John. O'M. Bokris and A.K.N.Reddy, "Modern Electrochemistry" vol 1, Plenum Press N.Y. 1970, chap.3.

46. J.Kirkwood, "Theory of Solutions (Gordon and Breach N.Y. 1968); J.Kirkwood and J.C. Poirier (ibid P 256).

47. R.Hastings, J. Chem. Phys., **68**, 675(1978).

48. J.P.Hansen, Phys. Rev., **A 8**, 3096(1973).

49. P. Vieillefosse and J.P.Hansen, Phys. Rev., **A 12**, 1106(1975).

50. L.D.Landau and E.M.Lifshitz, "Statistical Physics", Pergamon Press,

London 1958.

51. G.Stell, K.C.Wu and B.Larsen, Phys. Rev. Lett., **37**, 1369(1976).

52. M.Rovere, R.Miniero, M.Parrinello and M.P.Tosi, Phys. Chem. Liquid., **9**, 11(1979).

53. P.V.Giquinta, M.Parrinello and M.P.Tosi, Phys. Chem. Liquid, **5**, 305(1976).

54. L.Belloni, Phys. Rev. Lett., **57**, 2026(1986).

55. I.Sogami, Phys. Lett., **A 96**, 199(1983).

56. I.Sogami and N.Ise, J. Chem. Phys., **81**, 6320(1984).

57. J.Th.G.Overbeek, J. Chem. Phys., **87**, 4406(1987).

58. M.Born and R.OOppenheimer, Ann. Phys. (Leipzig) **84**, 457(1927).

59. L.D.Landau and E.M.Lifshitz, "Statistical Physics", Pergamon Press, S **74**, **20**,1958.

60. D.Pines and Ph.Nozières, " The Theory of Quantum Liquid" W.A.Benjamin, Inc. N.Y., Amesterdam 1966.

61. A.Kose, M.Osaki, K.Takano, Y.Kobayashi and S.Hachisu, J. Colloid Interface Sci., **44**, 330(1973); N.Ise, T.Okubo, M.Sugimura, K. Ito and H.J.Nlte, J. Chem. Phys., **78**, 536(1983).

62. R.G.Palmer and J.D.Weeks, J. Chem. Phys., **58**, 4171(1973).

63. L.B.Bhuiyan and N.H.March, Phys. Chem. Liquids, **6**, 261(1977).

64. M.Parrinello and M.P.Tosi, Chem. Phys. Lett., **64**, 579(1979).

65. R.J.Baxter, J. Chem. Phys., **52**, 4559(1970).

66. L.Blum, Mol. Phys., **30**, 1529(1975).

67. L.Belloni, J. Chem. Phys., **88**, 5143(1988).

68. G.Zerah and J.P.Hansen, J. Chem. Phys., **84**, 2336(1986).